

Lepton mixing and charged lepton flavour violation from inverse seesaw with non-degenerate heavy states

F. P. Di Meglio and C. Hagedorn

Instituto de Física Corpuscular, CSIC and Universidad de Valencia, Edificio Institutos Investigación, Catedrático José Beltrán 2, 46980 Paterna, Spain

E-mail: francescopaolo.dimeglio@ific.uv.es, claudia.hagedorn@ific.uv.es

Abstract

We analyse an inverse seesaw scenario with 3+3 gauge singlets. The flavour structure is determined by a flavour symmetry, $\Delta(3n^2)$ or $\Delta(6n^2)$, n integer, and CP and their residual groups among charged leptons and the neutral states. For the latter, the Dirac mass matrix of the gauge singlets carries all non-trivial flavour structure. Consequently, the heavy sterile states form three pseudo-Dirac pairs which have in general distinct masses. We discuss the signal strength of different charged lepton flavour violating processes. Ensuring that the lepton mixing angles can be accommodated at the 3σ level or better, we find that the current bounds on the branching ratios of $\mu \rightarrow e\gamma$, $\mu \rightarrow 3e$, $\tau \rightarrow \ell\gamma$ and $\tau \rightarrow 3\ell$, $\ell = e, \mu$, as well as the rate of $\mu - e$ conversion in nuclei do not strongly constrain the considered parameter space, while the limits expected from the upcoming experiments Mu3E, COMET and Mu2e will have a relevant impact.

1 Introduction

Neutrino masses and the observed lepton mixing pattern, encoded in the Pontecorvo-Maki-Nakagawa-Sakata (PMNS) mixing matrix, are two observational facts that cannot be satisfactorily explained in the Standard Model (SM). For this reason, many extensions of the SM have been proposed that feature a mechanism for neutrino mass generation. Among the most known ones are the type-I [1–5], type-II [6–11] and type-III seesaw mechanisms [12]. If the involved couplings are of order one and no (generalised) lepton number is imposed, see e.g. [13–15], the new particles are expected to have masses (much) larger than a few TeV. In contrast, the inverse seesaw (ISS) mechanism [16–19] can explain the lightness of neutrinos with the help of particle masses in the reach of current (and near-future) experiments and sizeable couplings, since the smallness of neutrino masses originates from the small breaking of lepton number. Non-abelian discrete symmetries, also in combination with CP, have shown to be prime candidates to understand the peculiar properties of lepton mixing, in particular if these symmetries are broken to (distinct) residual groups among charged leptons and neutral states [20–22], see [23–28] for earlier works and [29–33] for reviews. Members of the series of groups $\Delta(3n^2)$ [34] and $\Delta(6n^2)$ [35], n integer, are examples for such non-abelian discrete symmetries. As is known [36], from these, combined with CP, four different types of lepton mixing patterns can be derived that correspond to Case 1), Case 2), Case 3 a) and Case 3 b.1), respectively. A concise description of their properties can be found in e.g. [37]. For further studies of lepton mixing from the groups $\Delta(3n^2)$ and $\Delta(6n^2)$ and CP, see e.g. [38–48].

In the current work, we consider an ISS mechanism with $3 + 3$ heavy sterile states, N_i and S_j , $i, j = 1, 2, 3$. As flavour group we use one of the groups $\Delta(3n^2)$ and $\Delta(6n^2)$ (together with an additional Z_3 symmetry $Z_3^{(\text{aux})}$), while the CP symmetry corresponds to an automorphism of the flavour group. The charged lepton mass matrix is determined by a residual Z_3 group such that it is diagonal and contains three free parameters encoding the charged lepton masses. The neutrino Yukawa coupling and the mass matrices fixing the mass spectrum of the heavy sterile states are instead subject to the residual group $G_\nu = Z_2 \times CP$. Three different minimal cases can be studied: option 1 for which only the Majorana mass matrix of the sterile states S_j breaks the original symmetry to G_ν [37], while for option 2 only the neutrino Yukawa coupling encodes the breaking to G_ν [49] and option 3 is characterised by a Dirac mass matrix coupling the heavy sterile states N_i and S_j that is only invariant under G_ν . Here, we analyse the phenomenology of the latter option, in particular the masses and mixing of the light and heavy neutral states as well as the signal strength of charged lepton flavour violation (cLFV) such as the branching ratio (BR) of $\mu \rightarrow e\gamma$ and the $\mu - e$ conversion rate (CR) in nuclei.

The remainder of the paper is organised as follows: section 2 contains an outline of the setup, in which the flavour and CP symmetries and the transformation properties of the different fields under these are presented as well as the residual symmetries of the different mass matrices are discussed and their form is shown. Results for the mass spectrum of the light neutrinos and the heavy sterile states can be found in section 3 together with the mixing of light and heavy sterile states. In section 4 the masses of the heavy sterile states and the BRs and CR of $\mu - e$ transitions are analytically investigated. Results of numerical scans for different examples of Case 1) through Case 3 b.1) are discussed in section 5. Furthermore, we briefly comment on the expected size of BRs of radiative and trilepton cLFV tau lepton decays. We compare the results obtained for option 3 with those for option 1, found in [37], and for option 2, see [49], in section 6. In section 7 we summarise. We collect supplementary plots in appendix A.

2 Setup

We employ as flavour symmetry G_f a member of the series of groups $\Delta(3n^2)$ and $\Delta(6n^2)$, n not divisible by three nor by four. Left-handed (LH) lepton doublets L_α , $\alpha = e, \mu, \tau$, as well as the singlets N_i and S_j , $i, j = 1, 2, 3$, transform as a triplet under G_f , which we specify further below. Right-handed (RH) charged leptons $\ell_{\alpha R}$ are instead singlets (all in $\mathbf{1}$) under this group. In order to

distinguish these a Z_3 symmetry $Z_3^{(\text{aux})}$ is used, i.e. $\ell_{eR} \sim 1$, $\ell_{\mu R} \sim \omega$ and $\ell_{\tau R} \sim \omega^2$ with $\omega = e^{\frac{2\pi i}{3}}$. All other fields are invariant under $Z_3^{(\text{aux})}$. The CP symmetry is chosen according to [20–22], see also [23–28], as automorphism of G_f .

As mentioned, the charged lepton mass matrix m_ℓ is diagonal with three independent entries, corresponding to m_e , m_μ and m_τ .¹ This can be achieved with a residual Z_3 symmetry that is the diagonal subgroup of the Z_3 symmetry, generated by the generator a of the flavour group (which is always diagonal itself, compare e.g. appendix A in [49]), and $Z_3^{(\text{aux})}$.

The Lagrangian relevant for the masses and the mixing of the neutral states reads as follows

$$-(y_D)_{\alpha i} \bar{L}_\alpha^c H N_i^c - (M_{NS})_{ij} \bar{N}_i S_j - \frac{1}{2} (\mu_S)_{kl} \bar{S}_k^c S_l + \text{h.c.} \quad (1)$$

with $\langle H \rangle \approx 174 \text{ GeV}$, being the vacuum expectation value (VEV) of the SM Higgs. With the neutrino Yukawa coupling matrix y_D we can define the Dirac mass matrix m_D , $m_D = y_D \langle H \rangle$. The mass matrices, m_D , M_{NS} and μ_S , are constrained in general by the residual symmetry G_ν . We are interested in studying minimal cases. Two of these, option 1 and 2, in which either μ_S or m_D are invariant under G_ν , while the other mass matrices possess the original symmetry, have already been scrutinised in the literature [37, 49]. For the remaining option, option 3, the form of the matrix M_{NS} is non-trivial in flavour space, while m_D and μ_S preserve the entire flavour group and CP. This option can be realised as follows: we assign the singlets S_j to the real, unfaithful irreducible representation $\mathbf{3}'$ such that μ_S non-zero is allowed in the limit of unbroken symmetries and its flavour structure is trivial,²

$$\mu_S = \mu_0 \begin{pmatrix} 1 & 0 & 0 \\ 0 & 0 & 1 \\ 0 & 1 & 0 \end{pmatrix} \quad \text{with } \mu_0 > 0. \quad (2)$$

LH lepton doublets L_α are assigned to a complex, faithful irreducible representation of G_f , called $\mathbf{3}$, such that lepton mixing is determined by the structure of G_f and its residual symmetries. As the Dirac mass matrix m_D should also be invariant under the original group, we assign the singlets N_i to $\mathbf{3}$ as well. Then, the form of m_D is – in the limit of unbroken G_f and CP – given by

$$m_D = y_0 \begin{pmatrix} 1 & 0 & 0 \\ 0 & 1 & 0 \\ 0 & 0 & 1 \end{pmatrix} \langle H \rangle \quad \text{with } y_0 > 0. \quad (3)$$

Since $N_i \sim \mathbf{3}$ and $S_j \sim \mathbf{3}'$, it is obvious that the matrix M_{NS} vanishes for unbroken G_f . It is, thus, the source of symmetry breaking among the neutral states. Its flavour structure is derived by requesting it to be invariant under the subgroup $G_\nu = Z_2 \times CP$. We denote as $Z(\mathbf{r})$ and $X(\mathbf{r})$ the generator of the Z_2 group and the CP transformation in the representation \mathbf{r} (which equals $\mathbf{3}$ for L_α and N_i and $\mathbf{3}'$ for S_j), respectively. Consequently, the conditions that M_{NS} has to fulfil are

$$Z(\mathbf{3})^\dagger M_{NS} Z(\mathbf{3}') = M_{NS} \quad \text{and} \quad X(\mathbf{3})^* M_{NS} X(\mathbf{3}') = M_{NS}^*. \quad (4)$$

The explicit form of the matrices $Z(\mathbf{3})$, $Z(\mathbf{3}')$, $X(\mathbf{3})$ and $X(\mathbf{3}')$ can be found in [50]. The form of M_{NS} is constrained to be

$$M_{NS} = \Omega(\mathbf{3}) R_{ij}(\theta_N) \text{diag}(M_1, M_2, M_3) P_{kl}^{ij} R_{kl}(-\theta_S) \Omega(\mathbf{3}')^\dagger \quad (5)$$

with the unitary matrices $\Omega(\mathbf{3})$ and $\Omega(\mathbf{3}')$ obeying

$$\Omega(\mathbf{3}) \Omega(\mathbf{3})^T = X(\mathbf{3}) \quad \text{and} \quad \Omega(\mathbf{3}') \Omega(\mathbf{3}')^T = X(\mathbf{3}'). \quad (6)$$

Furthermore, $R_{ij}(\theta_N)$ and $R_{kl}(-\theta_S)$ are two rotations in the (ij) - and (kl) -planes, fixed by the pair of degenerate eigenvalues of the matrices $Z(\mathbf{3})$ and $Z(\mathbf{3}')$ in the basis transformed by $\Omega(\mathbf{3})$

¹We always assume them to be ordered canonically.

²This form of μ_S arises, since complex representation matrices for $\mathbf{3}'$ are employed.

and $\Omega(\mathbf{3}')$, respectively. The permutation matrix P_{kl}^{ij} is only necessary, if these two planes do not coincide. The two angles θ_N and θ_S together with the three mass parameters M_1 , M_2 and M_3 are the five (real) parameters contained in the matrix M_{NS} . For each case, Case 1) through Case 3 b.1), we have different forms of $\Omega(\mathbf{3})$ and $\Omega(\mathbf{3}')$ as well as the rotation planes (ij) and (kl) , see [50].³ As can be seen in the next section, the three mass parameters M_1 , M_2 and M_3 correspond to the distinct masses of the three pseudo-Dirac pairs of heavy neutral states to a very high degree.

3 Masses and mixing of light and heavy sterile states

In the following, we study the masses and mixing of the neutral states arising from the diagonalisation,

$$\mathcal{U}^T \mathcal{M}_{\text{Maj}} \mathcal{U} = \text{diag}(m_1, m_2, m_3, m_4, \dots, m_9) , \quad (7)$$

of the nine-by-nine matrix \mathcal{M}_{Maj} ,

$$\mathcal{M}_{\text{Maj}} = \begin{pmatrix} 0 & m_D & 0 \\ m_D^T & 0 & M_{NS} \\ 0 & M_{NS}^T & \mu_S \end{pmatrix} , \quad (8)$$

written in the basis $(\nu_{\alpha L}, N_i^c, S_j)$, with the unitary nine-by-nine matrix \mathcal{U} ,

$$\mathcal{U} = \begin{pmatrix} \tilde{U}_\nu & S \\ T & V \end{pmatrix} . \quad (9)$$

The masses $m_{1,2,3}$ are those of the light neutrinos and $m_{4,\dots,9}$ of the six heavy sterile states, while \tilde{U}_ν is a three-by-three, S a three-by-six, T a six-by-three and V a six-by-six matrix. None of these are in general unitary.

With the form of μ_S , m_D and M_{NS} , see eqs. (2,3,5), and assuming that $|\mu_S| \ll |m_D| \ll |M_{NS}|$ [16–19], we first deduce the mass matrix of the heavy sterile states and their mass spectrum. We have to look at

$$\begin{pmatrix} 0 & M_{NS} \\ M_{NS}^T & \mu_S \end{pmatrix} \quad (10)$$

which is approximately diagonalised by the matrix V , i.e.

$$V^T \begin{pmatrix} 0 & M_{NS} \\ M_{NS}^T & \mu_S \end{pmatrix} V \approx \text{diag}(m_4, \dots, m_9) . \quad (11)$$

We get

$$V = \frac{1}{\sqrt{2}} \begin{pmatrix} i\Omega(\mathbf{3})^* R_{ij}(\theta_N) & \Omega(\mathbf{3})^* R_{ij}(\theta_N) \\ -i\Omega(\mathbf{3}') R_{kl}(\theta_S) (P_{kl}^{ij})^T & \Omega(\mathbf{3}') R_{kl}(\theta_S) (P_{kl}^{ij})^T \end{pmatrix} . \quad (12)$$

The masses of the heavy sterile states, that form pseudo-Dirac pairs, are given by

$$m_4 \approx m_7 \approx M_1 \quad , \quad m_5 \approx m_8 \approx M_2 \quad \text{and} \quad m_6 \approx m_9 \approx M_3 . \quad (13)$$

These are splitted among each other by terms of order μ_0 . Indeed, if the combination

$$P_{kl}^{ij} R_{kl}(-\theta_S) \Omega(\mathbf{3}')^T \begin{pmatrix} 1 & 0 & 0 \\ 0 & 0 & 1 \\ 0 & 1 & 0 \end{pmatrix} \Omega(\mathbf{3}') R_{kl}(\theta_S) (P_{kl}^{ij})^T \quad (14)$$

is diagonal, the masses of the heavy sterile states read

$$m_4 \approx M_1 - \frac{\mu_0}{2} \quad , \quad m_7 \approx M_1 + \frac{\mu_0}{2} \quad , \quad m_5 \approx M_2 - \frac{\mu_0}{2} \quad , \quad m_8 \approx M_2 + \frac{\mu_0}{2} \quad , \quad m_6 \approx M_3 - \frac{\mu_0}{2} \quad , \quad m_9 \approx M_3 + \frac{\mu_0}{2} . \quad (15)$$

³We note that the form of M_{NS} is exactly the same as the one of the neutrino Yukawa coupling matrix in [50].

If the combination in eq. (14) is not diagonal, but only block-diagonal, then only the masses of one pair of pseudo-Dirac particles can be written in this form. For e.g. Case 1), it is

$$m_5 \approx M_2 - \frac{\mu_0}{2}, \quad m_8 \approx M_2 + \frac{\mu_0}{2}, \quad (16)$$

while the other masses are – up to the first order in μ_0 –

$$m_4 \approx M_1 - \frac{\mu_0}{2} \cos 2\theta_S, \quad m_7 \approx M_1 + \frac{\mu_0}{2} \cos 2\theta_S, \quad m_6 \approx M_3 + \frac{\mu_0}{2} \cos 2\theta_S, \quad m_9 \approx M_3 - \frac{\mu_0}{2} \cos 2\theta_S. \quad (17)$$

Coming to the leading order contribution to the light neutrino mass matrix m_ν [51],

$$m_\nu = m_D \left(M_{NS}^{-1} \right)^T \mu_S M_{NS}^{-1} m_D^T, \quad (18)$$

we see that it is of the form

$$m_\nu = y_0^2 \mu_0 \langle H \rangle^2 U_0(\theta_N)^* \text{diag}(M_1^{-1}, M_2^{-1}, M_3^{-1}) \left[\begin{array}{c} P_{kl}^{ij} R_{kl}(-\theta_S) \Omega(\mathbf{3}')^T \left(\begin{array}{ccc} 1 & 0 & 0 \\ 0 & 0 & 1 \\ 0 & 1 & 0 \end{array} \right) \Omega(\mathbf{3}') R_{kl}(\theta_S) (P_{kl}^{ij})^T \\ \text{diag}(M_1^{-1}, M_2^{-1}, M_3^{-1}) U_0(\theta_N)^\dagger \end{array} \right] \quad (19)$$

where we have used the definition

$$U_0(\theta) = \Omega(\mathbf{3}) R_{ij}(\theta). \quad (20)$$

Note that the expression in square brackets coincides with the one found in eq. (14) and it is decisive whether it is diagonal or block-diagonal. If it is diagonal, we arrive at

$$m_\nu = y_0^2 \mu_0 \langle H \rangle^2 U_0(\theta_N)^* \text{diag}(M_1^{-2}, M_2^{-2}, M_3^{-2}) U_0(\theta_N)^\dagger, \quad (21)$$

meaning that we can determine the mixing matrix \tilde{U}_ν ,

$$\tilde{U}_\nu^T m_\nu \tilde{U}_\nu \approx \text{diag}(m_1, m_2, m_3), \quad (22)$$

to be of the form

$$\tilde{U}_\nu \approx U_0(\theta_N) = \Omega(\mathbf{3}) R_{ij}(\theta_N) \quad (23)$$

and the light neutrino masses m_f , $f = 1, 2, 3$, are equal to

$$m_f = \frac{y_0^2 \mu_0 \langle H \rangle^2}{M_f^2}. \quad (24)$$

From eq. (23) and taking into account that the charged lepton mass matrix is diagonal with canonically ordered masses, meaning $U_\ell = \mathbb{1}$, the (non-unitary) PMNS mixing matrix reads the same as \tilde{U}_ν and the lepton mixing parameters only depend on the free parameter θ_N .

We remark that an additional permutation is necessary for Case 3 b.1), that requires a different assignment of the light neutrino masses,

$$m_1 = \frac{y_0^2 \mu_0 \langle H \rangle^2}{M_3^2}, \quad m_2 = \frac{y_0^2 \mu_0 \langle H \rangle^2}{M_1^2}, \quad m_3 = \frac{y_0^2 \mu_0 \langle H \rangle^2}{M_2^2}, \quad (25)$$

cf. [36, 49, 50]. For simplicity, we focus on Case 1) through Case 3 a) in the following, where this additional permutation is not needed for the lepton mixing pattern. However, all formulae can be easily also derived for Case 3 b.1) and all statements made hold analogously.

If the expression in eq. (14) is not diagonal, an additional rotation whose angle is fixed by two of the mass parameters M_f and the free angle θ_S is required, and it occurs in the same plane as $R_{ij}(\theta_N)$. So, we replace θ_N by an effective angle $\bar{\theta}_N$. At the same time, the light neutrino masses

m_f with $f = i$ or $f = j$ are not directly proportional to M_f^{-2} anymore, while the remaining mass still is.

The sub-leading contribution to the light neutrino mass matrix, m_ν^1 , in the expansion in powers of $(|m_D|/|M_{NS}|)$ [51], reads in general

$$m_\nu^1 = -\frac{1}{2} m_D \left(M_{NS}^{-1} \right)^T \left(\mu_S M_{NS}^{-1} m_D^T m_D^* \left(M_{NS}^{-1} \right)^\dagger + \left(M_{NS}^{-1} \right)^* m_D^\dagger m_D \left(M_{NS}^{-1} \right)^T \mu_S \right) M_{NS}^{-1} m_D^T. \quad (26)$$

It is convenient to rewrite m_ν^1 with the help of the (hermitean) matrix η which encodes the non-unitarity of the matrix \tilde{U}_ν (and, thus, of the PMNS mixing matrix), induced by the mixing of the light and heavy sterile states. It is defined as

$$\eta = \frac{1}{2} m_D^* \left(M_{NS}^{-1} \right)^\dagger M_{NS}^{-1} m_D^T, \quad (27)$$

and, consequently, m_ν^1 takes the form

$$m_\nu^1 = - (m_\nu \eta + \eta^* m_\nu). \quad (28)$$

Using m_D and M_{NS} as in eqs. (3,5), the matrix η is given by

$$\eta = \eta_0'' U_0(\theta_N) \text{diag}(M_1^{-2}, M_2^{-2}, M_3^{-2}) U_0(\theta_N)^\dagger, \quad (29)$$

where

$$\eta_0'' = \frac{y_0^2 \langle H \rangle^2}{2}. \quad (30)$$

So, the matrix m_ν^1 reads

$$m_\nu^1 = -2 \eta_0'' \tilde{U}_\nu^* \text{diag} \left(\frac{m_1}{M_1^2}, \frac{m_2}{M_2^2}, \frac{m_3}{M_3^2} \right) \tilde{U}_\nu^\dagger, \quad (31)$$

if the expression in eq. (14) is diagonal. In this situation, the sub-leading contribution does not affect the lepton mixing parameters and only slightly impacts the light neutrino masses.

If instead the combination in eq. (14) is non-diagonal, the matrix $U_0(\theta_N)$ appearing in η cannot be identified with \tilde{U}_ν , because $\tilde{U}_\nu \approx U_0(\bar{\theta}_N)$. However, we can still write η in terms of \tilde{U}_ν as

$$\eta = \eta_0'' \tilde{U}_\nu R_{ij}(\theta_N - \bar{\theta}_N) \text{diag}(M_1^{-2}, M_2^{-2}, M_3^{-2}) R_{ij}(\theta_N - \bar{\theta}_N)^T \tilde{U}_\nu^\dagger. \quad (32)$$

Then, we find

$$m_\nu^1 = -\eta_0'' \tilde{U}_\nu^* [\text{diag}(m_1, m_2, m_3) R_{ij}(\theta_N - \bar{\theta}_N) \text{diag}(M_1^{-2}, M_2^{-2}, M_3^{-2}) R_{ij}(\theta_N - \bar{\theta}_N)^T + \text{transpose}] \tilde{U}_\nu^\dagger, \quad (33)$$

meaning that this contribution introduces a small additional rotation in the (ij) -plane as well as small shifts in the light neutrino masses.

The (non-unitary) PMNS mixing matrix is of the form

$$\tilde{U}_{\text{PMNS}} = \tilde{U}_\nu = (\mathbb{1} - \eta) U_0. \quad (34)$$

For the expression in eq. (14) being diagonal, the matrix U_0 equals $U_0 = U_0(\theta_N)$ and using η as in eq. (29) we have

$$\tilde{U}_{\text{PMNS}} = U_0(\theta_N) (\mathbb{1} - \eta_0'' \text{diag}(M_1^{-2}, M_2^{-2}, M_3^{-2})). \quad (35)$$

We, thus, expect that the columns of the PMNS mixing matrix receive different suppression factors, since η_0'' is positive and the mass parameters M_f are in general different. Indeed, the latter can be expressed in terms of the light neutrino masses, see eq. (24).

If the expression in eq. (14) is not diagonal, the matrix U_0 in eq. (34) is $U_0 = U_0(\bar{\theta}_N)$ and, thus, we get

$$\tilde{U}_{\text{PMNS}} = U_0(\bar{\theta}_N) (\mathbb{1} - \eta_0'' R_{ij}(\theta_N - \bar{\theta}_N) \text{diag}(M_1^{-2}, M_2^{-2}, M_3^{-2}) R_{ij}(\theta_N - \bar{\theta}_N)^T). \quad (36)$$

Again, the correction acts differently on the different columns of the PMNS mixing matrix.

Eventually, we mention the form of S and T , that are computed – at leading order – as

$$S = \left(\mathbb{0} \quad , \quad m_D^* (M_{NS}^{-1})^\dagger \right) V \quad \text{and} \quad T = \begin{pmatrix} \mathbb{0} \\ -M_{NS}^{-1} m_D^T \tilde{U}_\nu \end{pmatrix}. \quad (37)$$

While the expression of S is always

$$S = \frac{y_0 \langle H \rangle}{\sqrt{2}} \left(-i U_0(\theta_N) \text{diag}(M_1^{-1}, M_2^{-1}, M_3^{-1}) \quad , \quad U_0(\theta_N) \text{diag}(M_1^{-1}, M_2^{-1}, M_3^{-1}) \right), \quad (38)$$

the form of the matrix T instead depends on whether the combination in eq. (14) is diagonal or not. For the diagonal case, we have

$$T = -y_0 \langle H \rangle \begin{pmatrix} \mathbb{0} \\ \Omega(\mathbf{3}') R_{kl}(\theta_S) (P_{kl}^{ij})^T \text{diag}(M_1^{-1}, M_2^{-1}, M_3^{-1}) \end{pmatrix}, \quad (39)$$

whereas for the non-diagonal case we find

$$T = -y_0 \langle H \rangle \begin{pmatrix} \mathbb{0} \\ \Omega(\mathbf{3}') R_{kl}(\theta_S) (P_{kl}^{ij})^T \text{diag}(M_1^{-1}, M_2^{-1}, M_3^{-1}) R_{ij}(\theta_N - \bar{\theta}_N)^T \end{pmatrix}. \quad (40)$$

4 Analytical estimates

In the following, we first estimate the expected size of the parameters y_0 , μ_0 and M_f of this scenario and then the signal strength of certain cLFV processes.

4.1 Estimates of parameters

To get an idea of the typical size of the Yukawa coupling y_0 and the scale μ_0 of lepton number violation and the relations among the mass parameters M_f , $f = 1, 2, 3$, we express these in terms of the light neutrino masses. We focus on the situation in which the combination in eq. (14) is diagonal and assume one of the cases Case 1) through Case 3 a) to be realised. From eq. (24), we have for light neutrino masses with normal ordering (NO)

$$M_1 = y_0 \langle H \rangle \sqrt{\frac{\mu_0}{m_0}}, \quad M_2 = y_0 \langle H \rangle \sqrt{\frac{\mu_0}{\sqrt{m_0^2 + \Delta m_{21}^2}}}, \quad M_3 = y_0 \langle H \rangle \sqrt{\frac{\mu_0}{\sqrt{m_0^2 + \Delta m_{31}^2}}}, \quad (41)$$

where m_0 is the lightest neutrino mass, while Δm_{21}^2 and Δm_{31}^2 are the solar and the atmospheric mass squared differences, respectively. We use the experimental best-fit values of the latter from [52] and take $m_0 = 0.03 \text{ eV}$, which is the maximal value of the lightest neutrino mass compatible with cosmological bounds on the sum of neutrino masses, see [53]. For mass parameters in the interval 150 GeV to 10 TeV, we estimate the size of y_0 and μ_0 to be

$$0.2 \lesssim y_0 \sqrt{\frac{\mu_0}{\text{eV}}} \lesssim 10. \quad (42)$$

Using the information on the light neutrino mass spectrum, we can also estimate the ratios of the mass parameters to be

$$\frac{M_1}{M_3} \approx 1.40 \quad \text{and} \quad \frac{M_2}{M_3} \approx 1.37. \quad (43)$$

For the lightest neutrino mass being zero, we see that M_1 becomes large, while the ratio of M_2 and M_3 tends to 2.41. These values agree well with the numerical results, see section 5. We display the dependence of the masses of the heavy sterile states on m_0 for fixed values of y_0 and μ_0 , $y_0 = 0.1$ and $\mu_0 = 3 \text{ keV}$, in the left of fig. 1.⁴

⁴The shown plots are produced by solving numerically for the eigenvalues and eigenvectors of the nine-by-nine matrix \mathcal{M}_{Maj} for a concrete choice of case, group theory parameters and CP symmetry that leads to the expression in eq. (14) being diagonal.

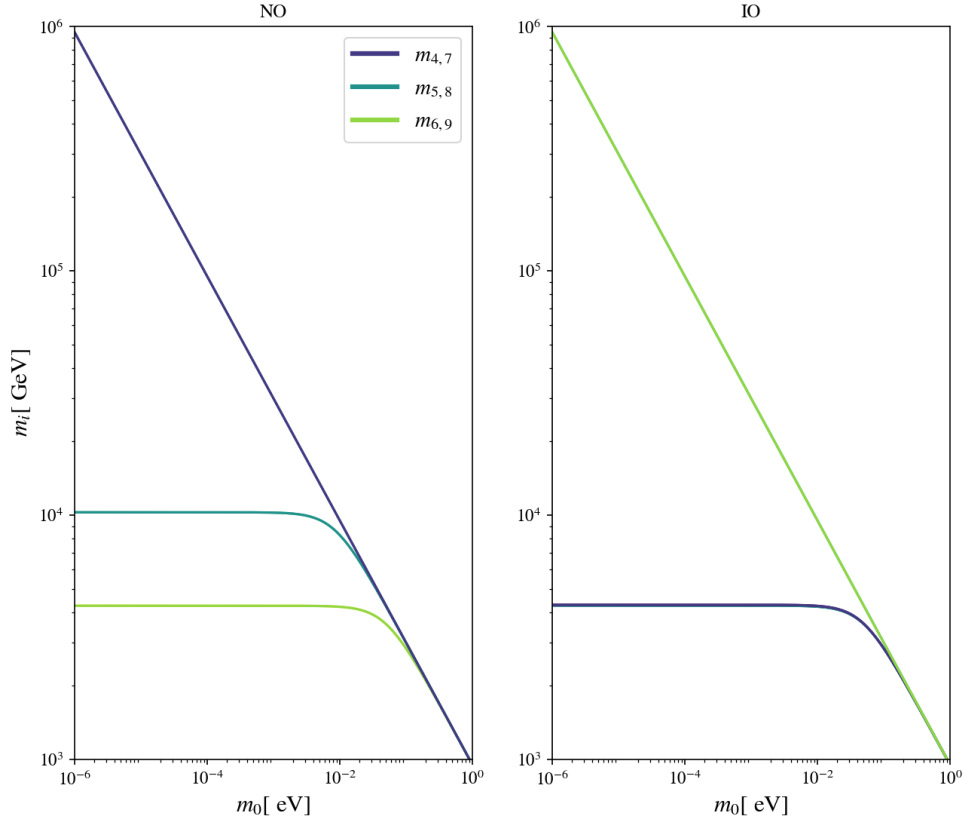


Figure 1: **Masses $m_{4,\dots,9}$ of the heavy sterile states in GeV as function of the lightest neutrino mass m_0 in eV.** In the left plot we display the results for light neutrino masses with NO and in the right plot for IO light neutrino masses. For concreteness, we fix $y_0 = 0.1$ and $\mu_0 = 3$ keV and use the best-fit values of the solar and the atmospheric mass squared differences from [52]. Note that the four masses m_4 , m_5 , m_7 and m_8 are almost degenerate in the case of an IO light neutrino mass spectrum, compare also eq. (46).

Similarly, we have for light neutrino masses with inverted ordering (IO)

$$M_1 = y_0 \langle H \rangle \sqrt{\frac{\mu_0}{\sqrt{m_0^2 + |\Delta m_{32}^2|} - \Delta m_{21}^2}}, \quad M_2 = y_0 \langle H \rangle \sqrt{\frac{\mu_0}{\sqrt{m_0^2 + |\Delta m_{32}^2|}}}, \quad M_3 = y_0 \langle H \rangle \sqrt{\frac{\mu_0}{m_0}}, \quad (44)$$

with Δm_{32}^2 denoting the atmospheric mass squared difference. We can perform an analogous estimate, employing $m_0 = 0.015$ eV as maximal value compatible with cosmological observations, and find

$$0.2 \lesssim y_0 \sqrt{\frac{\mu_0}{\text{eV}}} \lesssim 7. \quad (45)$$

Using this value for m_0 and the experimental best-fit values of the mass squared differences, we arrive at the ratios

$$\frac{M_1}{M_2} \approx 1.01 \quad \text{and} \quad \frac{M_3}{M_2} \approx 1.87. \quad (46)$$

In the limit m_0 being zero, M_3 becomes large, whereas the ratio of M_1 and M_2 remains approximately 1.01. The numbers are in agreement with the numerical results, found in section 5. The behaviour of the masses of the heavy sterile states with m_0 for fixed y_0 and μ_0 ($y_0 = 0.1$ and $\mu_0 = 3$ keV) is presented in the right of fig. 1.

4.2 Estimates for cLFV signals

For these estimates we make use of the formulae found in [54, 55]. As the heavy sterile states are in general not all (nearly) degenerate in mass, see preceding subsection, we cannot apply some of the simplifications employed for option 1 and 2.

We first consider the radiative cLFV decays $\ell_\beta \rightarrow \ell_\alpha \gamma$ whose BR is given by

$$\text{BR}(\ell_\beta \rightarrow \ell_\alpha \gamma) = \frac{\alpha_w^3 s_w^2}{256 \pi^2} \frac{m_\beta^4}{M_W^4} \frac{m_\beta}{\Gamma_\beta} \left| G_\gamma^{\beta\alpha} \right|^2, \quad (47)$$

where $\alpha_w = \frac{g_w^2}{4\pi}$ is the weak coupling, s_w the sine of the weak mixing angle, M_W the mass of the W boson, m_β the mass of the charged lepton of flavour β and Γ_β the corresponding total decay width. The form factor $G_\gamma^{\beta\alpha}$ reads

$$G_\gamma^{\beta\alpha} = \sum_{i=1}^{3+n_s} \mathcal{U}_{\alpha i} \mathcal{U}_{\beta i}^* G_\gamma(x_i), \quad (48)$$

where n_s is the number of the sterile states ($n_s = 6$), \mathcal{U} the unitary matrix defined in eq. (9), $x_i = \left(\frac{m_i}{M_W}\right)^2$ and $G_\gamma(x)$ is the loop function

$$G_\gamma(x) = -\frac{x(2x^2 + 5x - 1)}{4(1-x)^3} - \frac{3x^3}{2(1-x)^4} \log(x) \quad (49)$$

with $G_\gamma(0) = 0$ and the limit $G_\gamma(x) \approx \frac{1}{2}$ for $x \gg 1$. The contribution due to light neutrinos is negligible. Furthermore, we can use that the heavy sterile states form three pairs of pseudo-Dirac neutrinos, compare eq. (13), as well as the form of the matrix S in eq. (38). In this way, we can write the form factor $G_\gamma^{\beta\alpha}$ as

$$G_\gamma^{\beta\alpha} \approx 2\eta_0'' \left(U_0(\theta_N)_{\alpha 2} U_0(\theta_N)_{\beta 2}^* \left(\frac{G_\gamma(x_5)}{M_2^2} - \frac{G_\gamma(x_4)}{M_1^2} \right) + U_0(\theta_N)_{\alpha 3} U_0(\theta_N)_{\beta 3}^* \left(\frac{G_\gamma(x_6)}{M_3^2} - \frac{G_\gamma(x_4)}{M_1^2} \right) \right) \quad (50)$$

taking into account that $\alpha \neq \beta$. For larger masses of the heavy sterile states, i.e. larger than 3.3 TeV,⁵ the relative deviation of the loop function $G_\gamma(x)$ from 1/2 is less than one percent and we can safely approximate $G_\gamma(x)$ as 1/2 such that the expression for the form factor $G_\gamma^{\beta\alpha}$ simply reads

$$G_\gamma^{\beta\alpha} \approx \eta_{\alpha\beta}. \quad (51)$$

Consequently, the BR of $\ell_\beta \rightarrow \ell_\alpha \gamma$ is proportional to $|\eta_{\alpha\beta}|^2$, as has also been found for option 2 [49]. These formulae can be used in order to estimate the size of the BR of $\mu \rightarrow e \gamma$ for each case. For Case 1) and assuming $\theta_S = 0$, such that the matrix combination in eq. (14) is diagonal and the angle θ_N can be written in terms of the reactor mixing angle, cf. [36, 37], we obtain

$$G_\gamma^{\mu e} \approx 2\eta_0'' \left(\frac{1}{3} \left(\frac{G_\gamma(x_5)}{M_2^2} - \frac{G_\gamma(x_4)}{M_1^2} \right) - \frac{1}{2} \sin \theta_{13} \left(\sin \theta_{13} + \sqrt{2 - 3 \sin^2 \theta_{13}} \right) \left(\frac{G_\gamma(x_6)}{M_3^2} - \frac{G_\gamma(x_4)}{M_1^2} \right) \right). \quad (52)$$

We note that the expression does not depend on the parameter s that characterises the CP symmetry. Using $y_0 = 0.1$, $\mu_0 = 3$ keV and the best-fit values of the two mass squared differences and the reactor mixing angle, the BR of the decay $\mu \rightarrow e \gamma$ is estimated as

$$\text{BR}(\mu \rightarrow e \gamma) \approx 6.6 \times 10^{-16} (1.6 \times 10^{-15}) \quad (53)$$

for light neutrino masses with NO (IO) and $m_0 = 0.03$ eV ($m_0 = 0.015$ eV). Fig. 2 shows for Case 1) ($n = 26$ and $s = 1$), different values of the angle θ_S and light neutrino masses with NO and IO the results for the BRs of $\mu \rightarrow e \gamma$ and $\mu \rightarrow 3e$ as well as the CR of $\mu - e$ conversion in aluminium for fixed μ_0 , $\mu_0 = 3$ keV. The grey-shaded areas indicate the expected reach of the experiments MEG II, Mu3E (Phase 1 and Phase 2) and COMET, respectively (see also section 5.1). The values

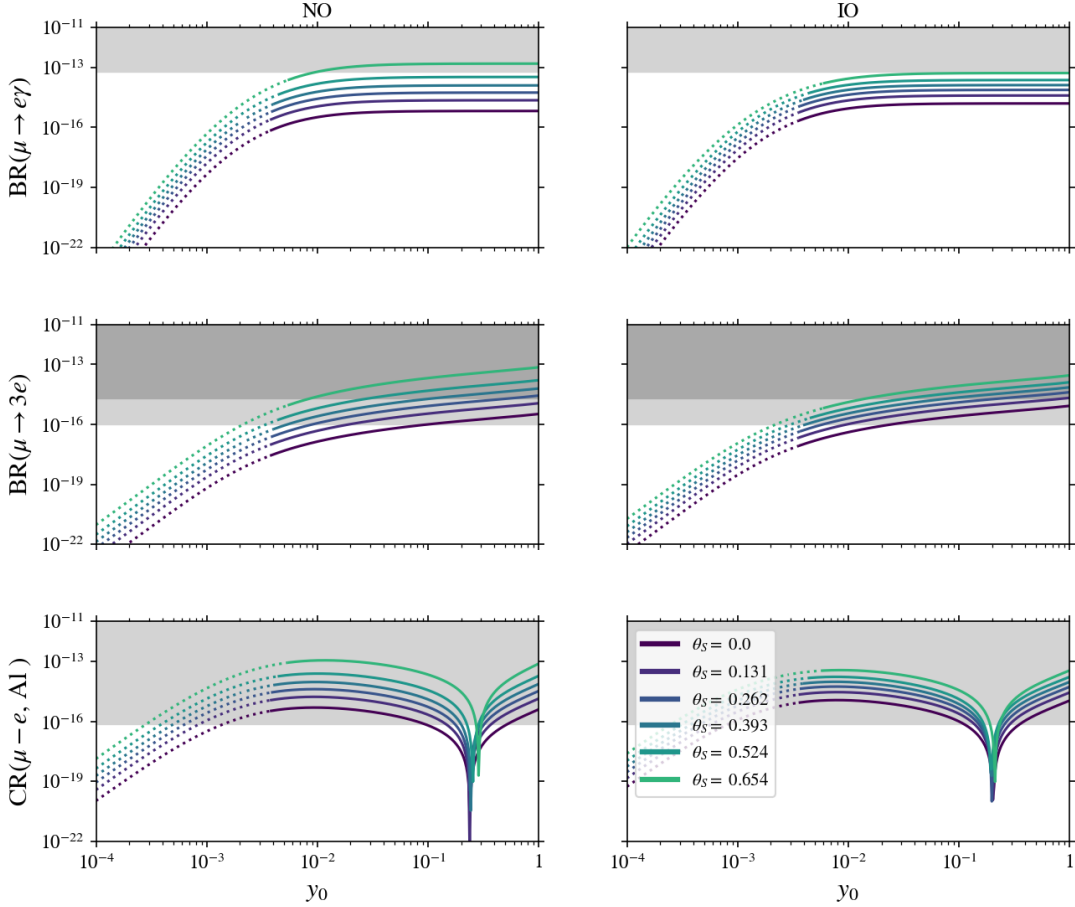
Case 1), $n=26, s=1$ 

Figure 2: **Case 1).** Results for $\text{BR}(\mu \rightarrow e \gamma)$, $\text{BR}(\mu \rightarrow 3e)$ and $\text{CR}(\mu - e, \text{AI})$ in the upper, middle and lower row, respectively. These results are for $n = 26$ and $s = 1$, and six different values of the angle θ_S , shown in different colours. In the left plot we display the results for light neutrino masses with NO and $m_0 = 0.03 \text{ eV}$ and in the right plot for IO light neutrino masses with $m_0 = 0.015 \text{ eV}$. For concreteness, we fix $\mu_0 = 3 \text{ keV}$ and use the best-fit values of the solar and the atmospheric mass squared differences and the reactor mixing angle [52]. The dotted lines indicate that at least one of the heavy sterile states has a mass lower than 150 GeV .

in eq. (53) agree well with those displayed in fig. 2. Similar estimates can be obtained for the other cases. Also the BRs of the trilepton cLFV decays $\ell_\beta \rightarrow 3 \ell_\alpha \gamma$ can be analysed in an analogous way.

More interesting is the consideration of the CR of $\mu - e$ conversion, since we can investigate whether or not it is still possible to obtain an exact cancellation of the CR for certain values of the parameters, in particular the value of the Yukawa coupling y_0 . Indeed, the CR can be written in the following form

$$\text{CR}(\mu - e, N) \propto \left| U_0(\theta_N)_{e2} U_0(\theta_N)_{\mu 2}^* \left(\frac{f(x_5)}{M_2^2} - \frac{f(x_4)}{M_1^2} \right) + U_0(\theta_N)_{e3} U_0(\theta_N)_{\mu 3}^* \left(\frac{f(x_6)}{M_3^2} - \frac{f(x_4)}{M_1^2} \right) \right|^2, \quad (54)$$

very similar to the expression for the BR of $\ell_\beta \rightarrow \ell_\alpha \gamma$, cf. eq. (50). The real-valued function $f(x)$ contains not only the nuclear form factors D , $V^{(n)}$ and $V^{(p)}$ of the nucleus N , s_w^2 and the electric charge e , but also loop functions. Here, it is only relevant that in the limit $x \gg 1$, $f(x)$ goes to zero

⁵This also holds for the numerical example in eq. (53).

for

$$x_0 = \exp \left(\frac{\frac{9}{8} V(n) + \left(\frac{9}{8} + \frac{37 s_w^2}{12} \right) V(p) - \frac{s_w^2}{16 e} D}{\frac{3}{8} V(n) + \left(\frac{4 s_w^2}{3} - \frac{3}{8} \right) V(p)} \right), \quad (55)$$

compare [54]. The CR can vanish, if both the real and imaginary part of the expression in eq. (54) are zero. In case that neither the real nor the imaginary part of $U_0(\theta_N)_{e3} U_0(\theta_N)_{\mu 3}^*$ vanish, the relation

$$\rho = \frac{\operatorname{Re}(U_0(\theta_N)_{e2} U_0(\theta_N)_{\mu 2}^*)}{\operatorname{Re}(U_0(\theta_N)_{e3} U_0(\theta_N)_{\mu 3}^*)} = \frac{\operatorname{Im}(U_0(\theta_N)_{e2} U_0(\theta_N)_{\mu 2}^*)}{\operatorname{Im}(U_0(\theta_N)_{e3} U_0(\theta_N)_{\mu 3}^*)} \quad (56)$$

has to be fulfilled. Furthermore, assuming that the combination in eq. (14) is diagonal (either in general or because of a specific choice of the angle θ_S), we can deduce from the vanishing of the real part alone

$$x_4 = \exp \left(\frac{\frac{9}{8} V(n) + \left(\frac{9}{8} + \frac{37 s_w^2}{12} \right) V(p) - \frac{s_w^2}{16 e} D}{\frac{3}{8} V(n) + \left(\frac{4 s_w^2}{3} - \frac{3}{8} \right) V(p)} + \frac{\rho \frac{m_2}{m_1} \log \left(\frac{m_1}{m_2} \right) + \frac{m_3}{m_1} \log \left(\frac{m_1}{m_3} \right)}{1 + \rho - \rho \left(\frac{m_2}{m_1} \right) - \left(\frac{m_3}{m_1} \right)} \right) \quad (57)$$

for Case 1) through Case 3 a). For Case 3 b.1) instead, we have

$$x_4 = \exp \left(\frac{\frac{9}{8} V(n) + \left(\frac{9}{8} + \frac{37 s_w^2}{12} \right) V(p) - \frac{s_w^2}{16 e} D}{\frac{3}{8} V(n) + \left(\frac{4 s_w^2}{3} - \frac{3}{8} \right) V(p)} + \frac{\frac{m_1}{m_2} \log \left(\frac{m_2}{m_1} \right) + \rho \frac{m_3}{m_2} \log \left(\frac{m_2}{m_3} \right)}{1 + \rho - \left(\frac{m_1}{m_2} \right) - \rho \left(\frac{m_3}{m_2} \right)} \right) \quad (58)$$

due to the different relation between the light neutrino masses m_f and the three mass parameters, M_1 , M_2 and M_3 , compare eqs. (24) and (25). Eqs. (57) and (58) clearly show that the value of x_4 at which the cancellation occurs is shifted with respect to the result obtained for option 2, see eq. (55). In addition, we observe that the value of x_4 depends on the case considered (through ρ and the assignment of the light neutrino masses m_f and the three mass parameters). Expressing m_f in eqs. (57) and (58) in terms of the lightest neutrino mass m_0 and the two measured mass squared differences also reveals that the value of x_4 changes with these and, obviously, depends on the light neutrino mass ordering. In the limit in which m_0 is very small, e.g. $m_0 \lesssim 10^{-5}$ eV, the form of the expressions in eqs. (57) and (58) simplifies further. For Case 1) and using the best-fit values of the two mass squared differences and the reactor mixing angle and employing $s_w^2 = 0.23$, $\alpha_{\text{em}} = \frac{e^2}{4\pi} = \frac{1}{137}$ as well as the nuclear form factors for aluminium as found in [56], we obtain from eq. (57)

$$x_4 \approx 26829 (11033) \quad (59)$$

for light neutrino masses with NO (IO) and $m_0 = 0.03$ (0.015) eV. Using again eq. (24) and setting $\mu_0 = 3$ keV, we can derive the corresponding value for y_0

$$y_0 \approx 0.24 (0.20). \quad (60)$$

These values match well with the plots in the lower row of fig. 2. At least for light neutrino masses with NO a slight dependence on the value of the angle θ_S can be observed. Note that for Case 1) the imaginary parts of $U_0(\theta_N)_{e2} U_0(\theta_N)_{\mu 2}^*$ and $U_0(\theta_N)_{e3} U_0(\theta_N)_{\mu 3}^*$ are zero and, hence, the imaginary part of the expression in eq. (54) always vanishes. Depending on the case and also on the value of the lightest neutrino mass m_0 , in particular if m_0 is small, the value of y_0 is affected. Likewise, the choice of θ_S as well as the different values of θ_N , that lead to a fit of the lepton mixing angles within the experimentally preferred 3σ ranges [52], can impact the value of y_0 at which the cancellation occurs (e.g. for Case 3 a)). We also remark that even if an exact cancellation cannot happen, we encounter a minimum value of the CR for $\mu - e$ conversion in aluminium, e.g. for Case 2) compare figs. 8 and 9 in appendix A. Furthermore, we refer to the different figures showing results of the numerical scans, see section 5. However, in these the difference between an exact cancellation and a minimum in the CR for $\mu - e$ conversion in aluminium is difficult to observe.

Lastly, we comment on the possibility that a cancellation also occurs in (one of) the BRs. This could happen, since the masses of the heavy sterile states are in general not degenerate and the expressions for the BRs become more contrived. Nevertheless, such a cancellation is usually not observed in figs. 2,8,9 nor in the numerical scans, see section 5, as it typically requires values of the Yukawa coupling y_0 (compare eq. (61)) and/or values of the masses of the heavy sterile states (see below eq. (64)) that are not considered in this study, and/or values of the angle θ_N which do not lead to an acceptable fit of the experimental data on lepton mixing. Some suppression in the BRs of $\mu \rightarrow e\gamma$ and $\mu \rightarrow 3e$ can, however, be inferred in certain instances, compare e.g. fig. 10 in appendix A. Similar statements hold for the BRs of the cLFV tau lepton decays, $\tau \rightarrow e\gamma$, $\tau \rightarrow 3e$, $\tau \rightarrow \mu\gamma$ and $\tau \rightarrow 3\mu$, see section 5.3.

5 Numerical results

We first enumerate the experimental inputs and (current/future) constraints as well as the region of parameter space of the scenario studied numerically. Then, we discuss results for the most relevant $\mu - e$ transitions, the decays $\mu \rightarrow e\gamma$ and $\mu \rightarrow 3e$ as well as $\mu - e$ conversion in aluminium, for representatives of each case, Case 1) through Case 3 b.1). We also briefly comment on the cLFV tau lepton decays, $\tau \rightarrow e\gamma$, $\tau \rightarrow 3e$, $\tau \rightarrow \mu\gamma$ and $\tau \rightarrow 3\mu$.

5.1 Prerequisites

We summarise the experimental inputs and constraints that we apply together with the region of parameter space scrutinised numerically.

Experimental inputs and constraints. We employ the results of the global fit of the NuFIT collaboration for the best-fit values of the mass squared differences and the 3σ ranges of the lepton mixing angles [52]. Furthermore, we use the bound on the sum of the light neutrino masses from cosmology [53]. For the masses of the heavy sterile states, we require these to be at least 150 GeV, compare [57–71] for different phenomenological studies.

We use as bounds on the elements $\eta_{\alpha\beta}$, $\alpha, \beta = e, \mu, \tau$, those from [72]. The current limits on the $\mu - e$ transitions, i.e. the BR of $\mu \rightarrow e\gamma$ and $\mu \rightarrow 3e$ as well as the CR of $\mu - e$ conversion in gold and titanium, are taken from [73–76], respectively. As future bounds, we employ the one from MEG II for $\mu \rightarrow e\gamma$, $\text{BR}(\mu \rightarrow e\gamma) < 6 \times 10^{-14}$ [77], from Mu3E for $\mu \rightarrow 3e$, $\text{BR}(\mu \rightarrow 3e) < 20(1) \times 10^{-16}$ Phase 1 (2) [78], as well as from COMET (Mu2e) for $\mu - e$ conversion in aluminium, $\text{CR}(\mu - e, \text{Al}) < 7(8) \times 10^{-17}$ [79–82], respectively.

For the BRs of the four cLFV tau lepton decays that we study we use the current limits from Belle [83, 84], Belle II [85] and LHCb [86]. Prospective bounds on these BRs from Belle II, between a few times 10^{-10} and a few times 10^{-9} , can be found in [87].

Region of parameter space considered. The parameter space of the neutral states comprises the Yukawa coupling y_0 , the mass scale μ_0 of lepton number violation, the three mass parameters M_f , $f = 1, 2, 3$, as well as the two angles θ_N and θ_S . We consider as range of y_0

$$10^{-4} \leq y_0 \leq 1, \quad (61)$$

while the scale μ_0 is varied in the interval⁶

$$100 \text{ eV} \leq \mu_0 \leq 1 \text{ MeV}. \quad (62)$$

Both of these quantities are varied logarithmically in their intervals. We note that viable data points are found for $y_0 \gtrsim 2 \times 10^{-4}$, with the exact value slightly depending on the case considered, since only then the masses of the heavy sterile states are larger than 150 GeV (and also all employed experimental constraints are satisfied). Likewise, the scale μ_0 is constrained to fulfil $\mu_0 \gtrsim 2 \text{ keV}$ (with the exact value again depending on the case considered) in order to pass current limits on

⁶This range is slightly extended compared to the numerical scan performed for option 2 [49].

the magnitudes of the elements of the matrix η and the prospective bounds on the BRs of $\mu \rightarrow e\gamma$ and $\mu \rightarrow 3e$ as well as on $\text{CR}(\mu - e, \text{Al})$. These findings are reflected in figs. 3-13. Furthermore, the unconstrained angle θ_S , contained in M_{NS} , cf. eq. (5), can lie in its entire admitted range

$$0 \leq \theta_S \leq 2\pi, \quad (63)$$

which is scanned linearly in the numerical analysis. In contrast, the angle θ_N is fixed in such a way that the measured lepton mixing angles are accommodated best (and always in their experimentally preferred 3σ ranges) [52] and M_f , $f = 1, 2, 3$, are adjusted in order to correctly reproduce the assumed light neutrino mass spectrum, its ordering (NO or IO), the best-fit values of the solar and the atmospheric mass squared differences and the chosen benchmark value of the lightest neutrino mass. The latter corresponds either to the maximal value compatible with cosmological observations [53],

$$m_0 = 0.03 \text{ eV (NO) or } m_0 = 0.015 \text{ eV (IO)}, \quad (64)$$

or a benchmark value among the following ones, $m_0 = 10^{-3} \text{ eV}$, $m_0 = 10^{-5} \text{ eV}$, $m_0 = 10^{-8} \text{ eV}$, $m_0 = 10^{-11} \text{ eV}$ and $m_0 = 10^{-14} \text{ eV}$ – for both light neutrino masses with NO and IO. We remark, however, that for $m_0 \lesssim 10^{-5} \text{ eV}$ the resulting plots look identical. We, thus, choose the value $m_0 = 10^{-5} \text{ eV}$. In this way, we typically get masses for the heavy sterile states ranging between 150 GeV and 700 TeV, with the upper value increasing with smaller values of m_0 .

For certain plots, see e.g. fig. 1, and numerical estimates, compare eq. (53) for example, we use as benchmark $y_0 = 0.1$ and $\mu_0 = 3 \text{ keV}$.

The numerical scans are performed in an analogous way as in the study of option 2, cf. details in appendix C of [49].

5.2 Scans for $\mu - e$ transitions

We discuss representative examples for each case in turn and present corresponding plots. For all shown examples the lepton mixing angles are accommodated at least at the 3σ level [52]. In order to facilitate the comparison between the results obtained for option 3 and those for option 2 [49], we employ the same examples.

The colour-coding of the data points in the plots, e.g. fig. 3, is as follows: for grey points at least one of the future limits on $\text{BR}(\mu \rightarrow e\gamma)$, $\text{BR}(\mu \rightarrow 3e)$ or $\text{CR}(\mu - e, \text{Al})$ is violated as well as the current bound on at least one of the elements of the matrix η . In the case of orange points at least one of the future limits is violated, but all current constraints on the magnitude of the matrix elements $\eta_{\alpha\beta}$ are fulfilled, while red points represent data points that are excluded by the current bounds on $\eta_{\alpha\beta}$, but not by the prospective limits on the three studied $\mu - e$ transitions. The different colours that can be read off from the colour bar in the plot indicate the minimum of the masses $m_{4,\dots,9}$ of the heavy sterile states for each viable data point which satisfies both the expected bounds on the mentioned cLFV processes and the current limits on $\eta_{\alpha\beta}$.

Case 1) As representative we use

$$n = 26 \text{ and } s = 1, \quad (65)$$

noting that the particular choice of s , the CP symmetry, is not relevant. The results for light neutrino masses with NO and $m_0 = 0.03 \text{ eV}$ are reported in fig. 3. Those for IO light neutrino masses look very similar and, thus, are omitted. We observe that the BR of $\mu \rightarrow e\gamma$ turns out to be smaller than about 6×10^{-16} , in case current bounds on the elements of the matrix η and future limits on the three $\mu - e$ transitions are taken into account. A lower limit does not seem to exist. The results for $\text{BR}(\mu \rightarrow 3e)$ show that also this BR can be (very) suppressed, while its maximum for viable data points (coloured according to the colour bar) is 10^{-16} , meaning that the prospective limit from Mu3E Phase 2 is effective. Analogous conclusions hold for $\text{CR}(\mu - e, \text{Al})$, i.e. (exact) cancellation in the CR is possible and the maximum value for viable data points is determined by the expected bound coming from COMET. Furthermore, we find that the signal strength of

Case 1), $n=26, s=1$, NO

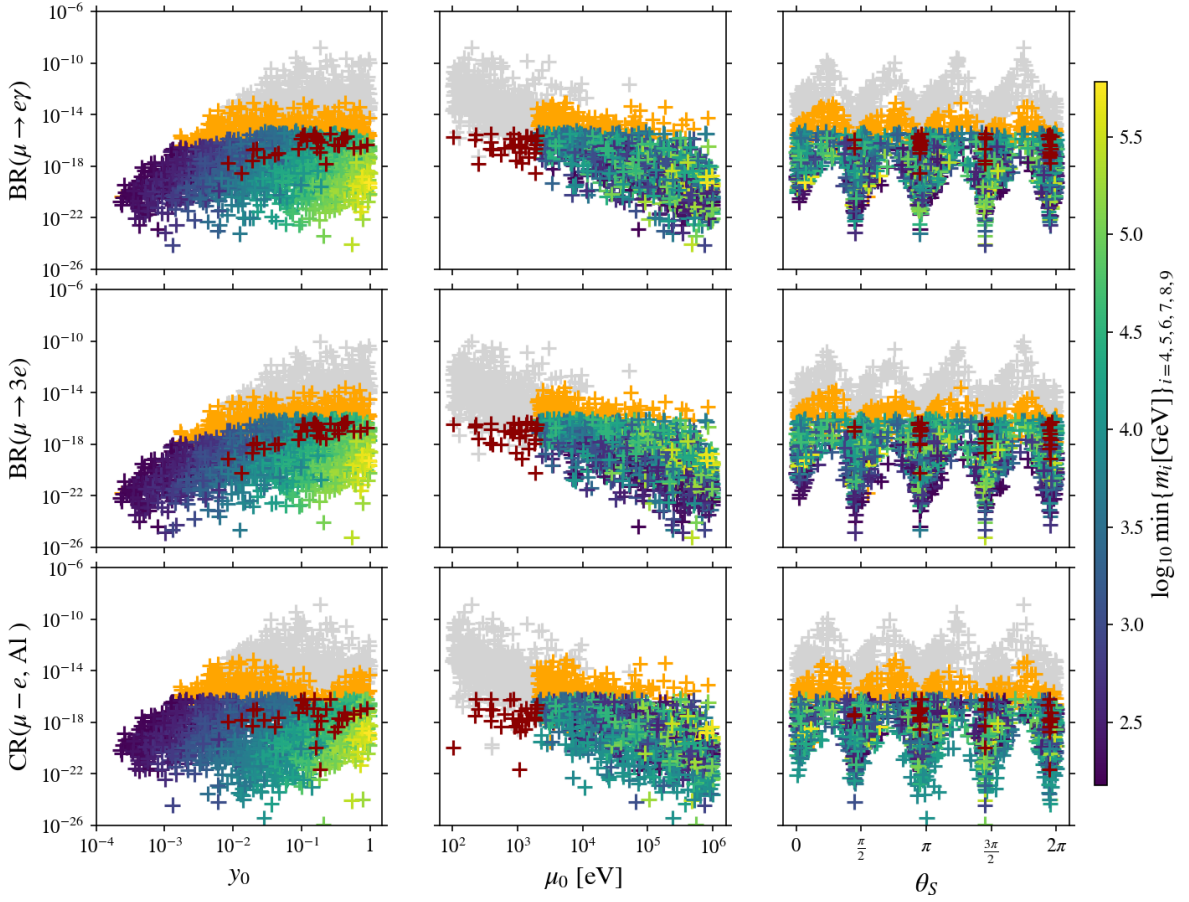


Figure 3: **Case 1).** Results of numerical scan for $\text{BR}(\mu \rightarrow e\gamma)$, $\text{BR}(\mu \rightarrow 3e)$ and $\text{CR}(\mu - e, \text{Al})$ varying y_0 , μ_0 and θ_S in the ranges in eqs. (61), (62) and (63), respectively. The parameters n and s are the same as in fig. 2. The light neutrino mass ordering is fixed to NO and m_0 to $m_0 = 0.03 \text{ eV}$. Points in grey, orange and red are excluded by different (current/future) experimental bounds, see text for details. Points in other colours correspond to a certain value of the lightest mass of the heavy sterile states, see colour bar, and pass all the imposed limits.

the studied $\mu - e$ transitions is enhanced for θ_S satisfying $\cos 2\theta_S \approx 0$. On the other hand, for $|\cos 2\theta_S|$ close to one, the BRs and CR become (strongly) suppressed. Considering smaller values of the lightest neutrino mass m_0 , e.g. $m_0 = 10^{-5} \text{ eV}$, can lead to variations in the dependence of the BRs and CR on the angle θ_S , compare fig. 10 for light neutrino masses with IO in appendix A. Additionally, it seems to be more unlikely to obtain strongly suppressed values of the two BRs.

Case 2) We choose as representatives

$$n = 14 \text{ and } (s, t) = (1, 1), (1, 2), (0, 1) \quad (66)$$

corresponding to $u = 1, 0, -1$ (and $v = 3, 6, 3$), respectively, since s and t , that characterise the CP symmetry, are related to u (and v) by $u = 2s - t$ (and $v = 3t$), cf. [36]. The most striking difference between the various choices of s and t is the fact that for t odd (u odd) the BRs and CR reveal a dependence on the angle θ_S , while this is not the case for t even (u even). This is due to the fact that for t even (u even) the combination in eq. (14) is diagonal, whereas it is only block-diagonal for t odd (u odd), see also [50]. Given this difference we display results for both $u = 0$ (i.e. for $s = 1$ and $t = 2$) and $u = 1$ (i.e. for $s = 1$ and $t = 1$) in figs. 4 and 5 for NO

Case 2), $n = 14, s = 1, t = 2 (u = 0)$, NO

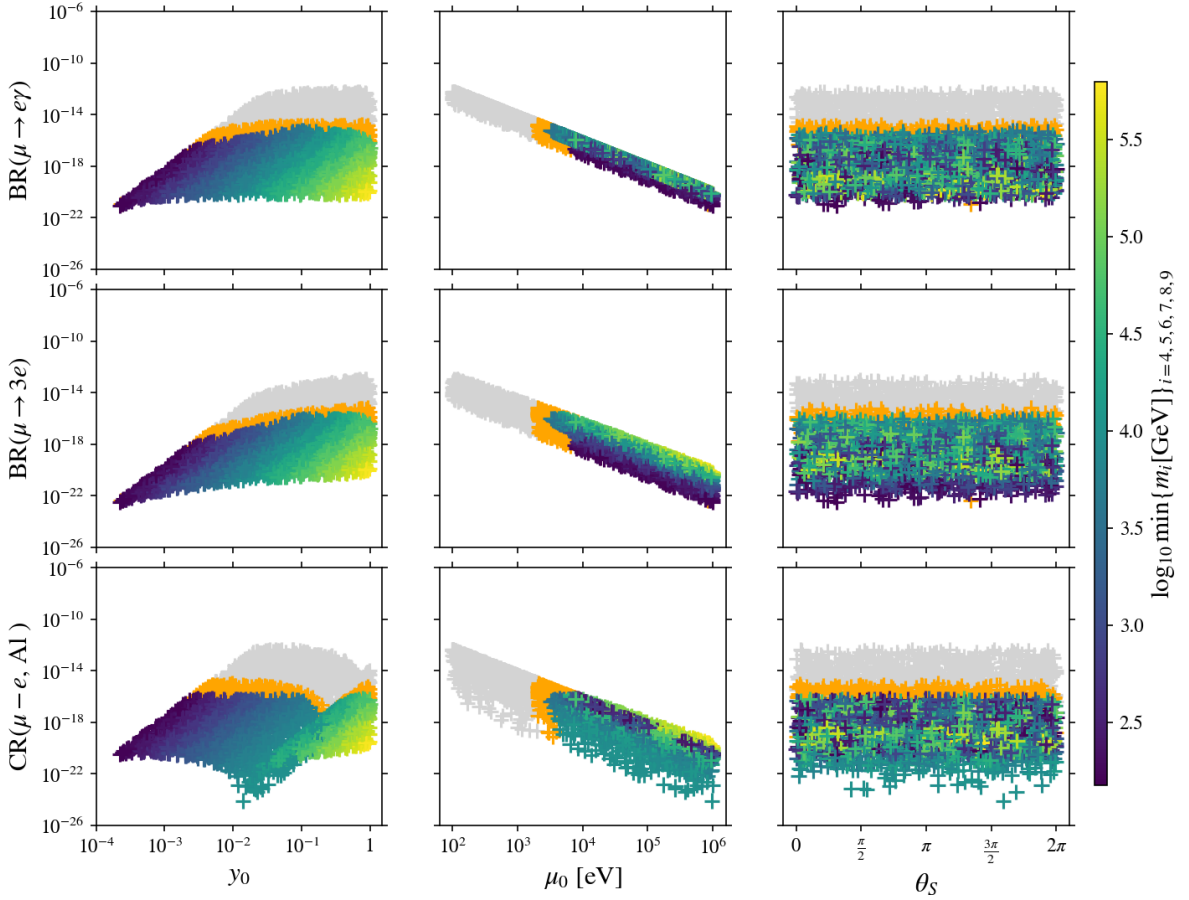


Figure 4: **Case 2).** Results of numerical scan for $\text{BR}(\mu \rightarrow e\gamma)$, $\text{BR}(\mu \rightarrow 3e)$ and $\text{CR}(\mu - e, \text{Al})$ varying y_0 , μ_0 and θ_S in the ranges in eqs. (61), (62) and (63), respectively. The parameters n , s and t are set to $n = 14$, $s = 1$ and $t = 2$ corresponding to $u = 0$ (and $v = 6$). The light neutrino mass ordering is fixed to NO and m_0 to $m_0 = 0.03 \text{ eV}$. The colour-coding of the data points is the same as in fig. 3.

light neutrino masses and $m_0 = 0.03 \text{ eV}$. As one can clearly see, in the latter case the BRs and CR are enhanced for $\sin 2\theta_S \approx 0$ and suppressed for the magnitude of $\sin 2\theta_S$ being close to one. This dependence on θ_S should be contrasted with the one observed for Case 1). Furthermore, we find that the largest possible values of the BRs and CR for viable data points are very similar for Case 1) and Case 2), whereas for Case 2) $\text{BR}(\mu \rightarrow e\gamma)$ and $\text{BR}(\mu \rightarrow 3e)$ appear to always have values larger than 10^{-21} and 10^{-23} , respectively. For the choice $u = -1$ hold the same statements as for $u = 1$. Furthermore, IO light neutrino masses lead to similar results. For a smaller value of m_0 , $m_0 = 10^{-5} \text{ eV}$, the obtained results are similar to those presented, with the tendency to render suppressed values of the BRs and CR less likely. We note that in all plots both values of the angle θ_N that allow for a good fit of the measured lepton mixing angles are used and no difference between them is found, when scanning y_0 , μ_0 and θ_S in the ranges in eqs. (61), (62) and (63), respectively. Yet, in plots with a fixed value of μ_0 slight differences are encountered, compare figs. 8 and 9 in appendix A. In such plots, also the fact that $\text{CR}(\mu - e, \text{Al})$ is only suppressed, but there exists no exact cancellation for Case 2) can be seen, which is not visible well in the numerical scans.

Case 3 a) Representatives of this case are

$$n = 34, \quad m = 2 \quad \text{and} \quad s = 1, 2. \quad (67)$$

Case 2), $n = 14, s = 1, t = 1 (u = 1)$, NO

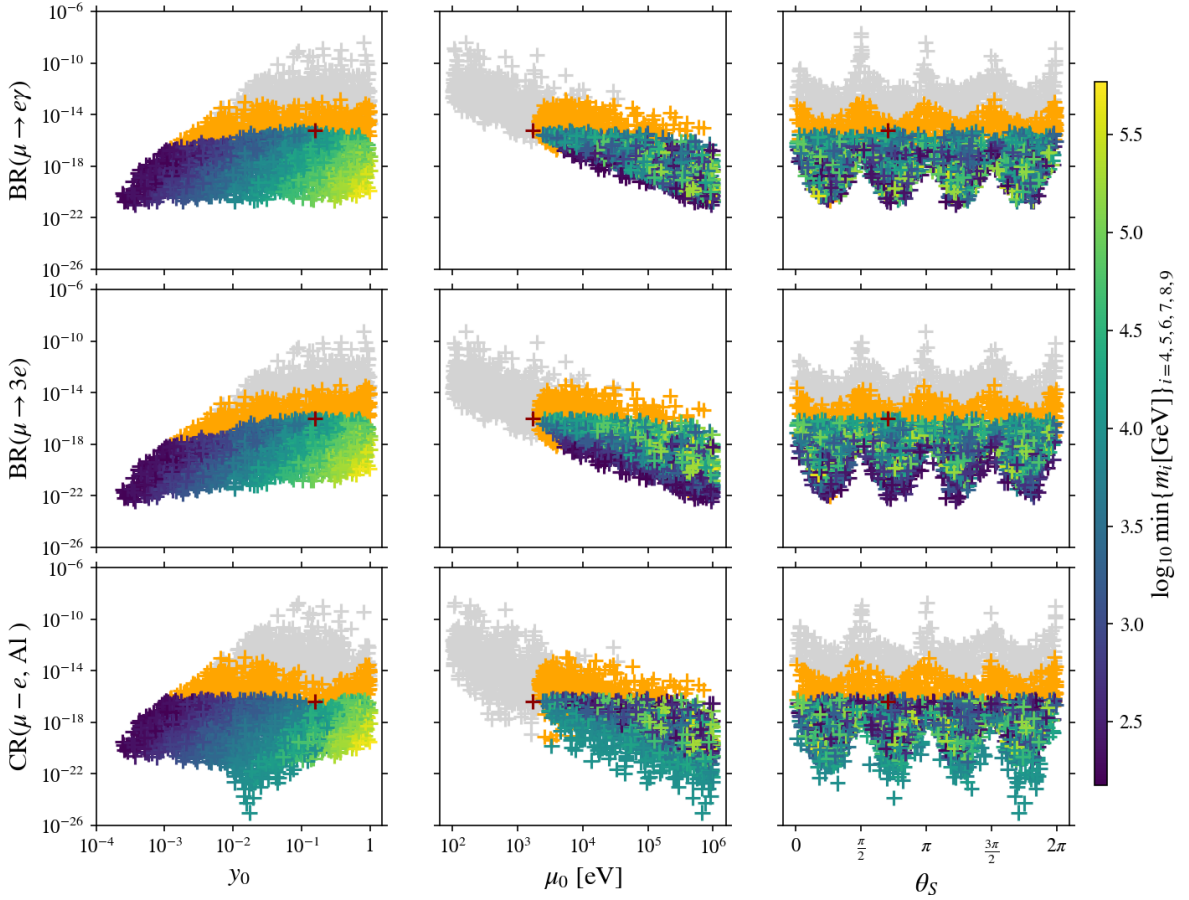


Figure 5: **Case 2).** Results of numerical scan for $\text{BR}(\mu \rightarrow e\gamma)$, $\text{BR}(\mu \rightarrow 3e)$ and $\text{CR}(\mu - e, \text{AI})$ varying y_0 , μ_0 and θ_S in the ranges in eqs. (61), (62) and (63), respectively. The parameters n , s and t are set to $n = 14$, $s = 1$ and $t = 1$ corresponding to $u = 1$ (and $v = 3$). The light neutrino mass ordering is fixed to NO and m_0 to $m_0 = 0.03 \text{ eV}$. The colour-coding of the data points is the same as in fig. 3.

Like for Case 2), we find that the combination of the parameters m (determining the generator of the residual Z_2 symmetry among the neutral states) and s (corresponding to the CP symmetry) fixes the dependence on the angle θ_S , i.e. for m and s being both even or odd the BRs and CR do not depend on θ_S , whereas for m even and s odd (or vice versa, as possible for a different choice of the index n) the BRs and CR depend on $\cos 2\theta_S$, meaning for $\cos 2\theta_S \approx 0$ their values are enhanced and suppressed for $|\cos 2\theta_S| \approx 1$. This is very similar to what is observed for Case 1). Since the plots for $m = 2$ and $s = 2$ and m_0 fixed as in eq. (64) look similar to the analogous plots for Case 2) ($n = 14, s = 1, t = 2$), see fig. 4, we refrain from displaying them. Instead, we show in fig. 6 results for $m = 2$ and $s = 1$ and NO light neutrino masses with $m_0 = 0.03 \text{ eV}$. Although a dependence on the angle θ_S is expected, it is hardly visible, compared to Case 1) in fig. 3 and Case 2) in fig. 5. When considering light neutrino masses with IO similar results are found. Only for smaller values of m_0 , $m_0 = 10^{-5} \text{ eV}$, and NO light neutrino masses the dependence of the BRs and CR on θ_S becomes more pronounced, see fig. 11 in appendix A. In addition, we note the peculiar feature that two branches in the scan results are visible (for small values of y_0) which correspond to the two different choices of the angle θ_N that lead to an agreement with the measured values of the lepton mixing angles at the 3σ level or better. This is best seen in fig. 12, also found in the appendix. Regarding the size of the BRs and CR, like for Case 2) the BRs typically observe as lower limits $\text{BR}(\mu \rightarrow e\gamma) \gtrsim 10^{-21}$ and $\text{BR}(\mu \rightarrow 3e) \gtrsim 10^{-23}$, while the CR can, in principle, be very suppressed.

Case 3 a), $n=34, m=2, s=1, \text{NO}$

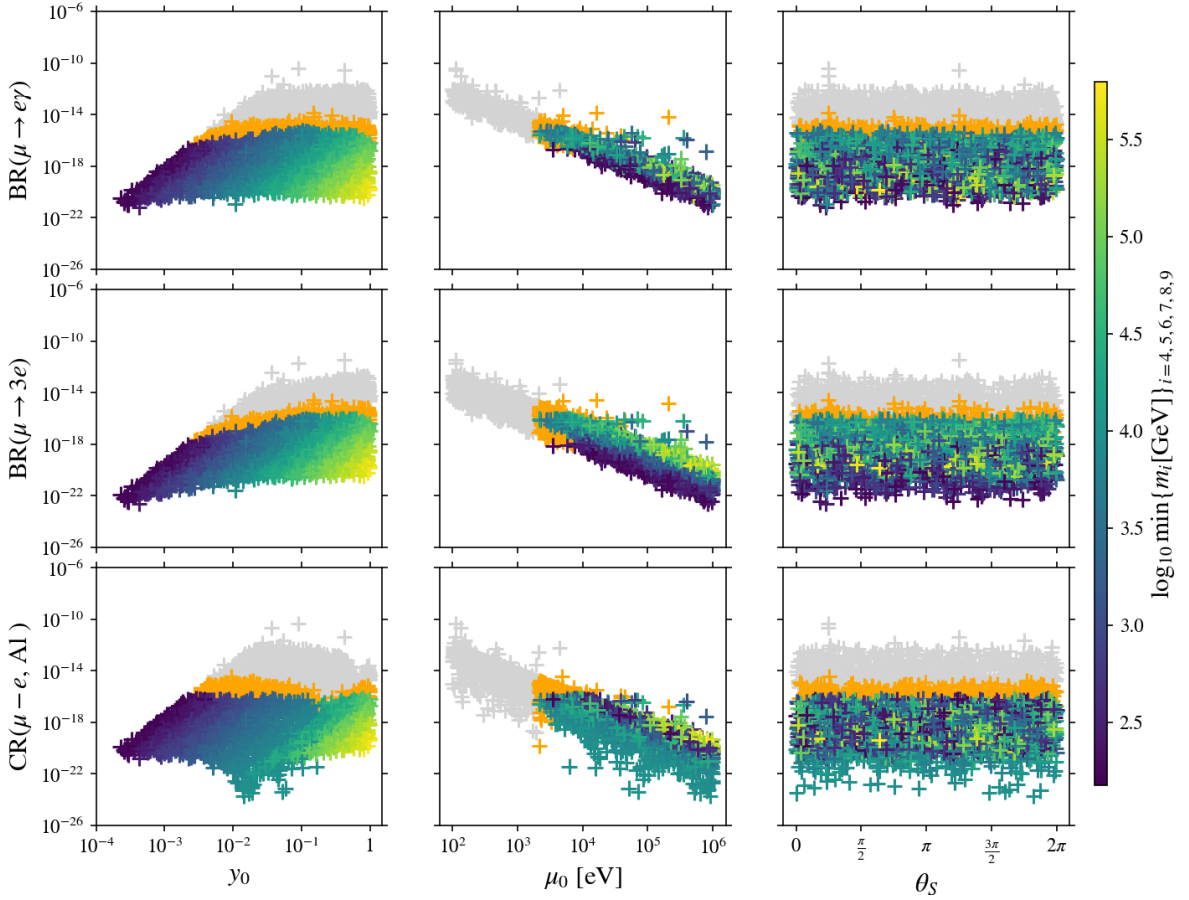


Figure 6: **Case 3 a).** Results of numerical scan for $\text{BR}(\mu \rightarrow e\gamma)$, $\text{BR}(\mu \rightarrow 3e)$ and $\text{CR}(\mu - e, \text{AI})$ varying y_0 , μ_0 and θ_S in the ranges in eqs. (61), (62) and (63), respectively. The parameters n , m and s are set to $n = 34$, $m = 2$ and $s = 1$. The light neutrino mass ordering is fixed to NO and m_0 to $m_0 = 0.03 \text{ eV}$. The colour-coding of the data points is the same as in fig. 3.

Furthermore, we find for the viable data points very similar maximal values that the BRs and CR attain as in Case 1) and Case 2).

Case 3 b.1) For this case we have analysed different combinations with

$$n = 20, \quad m = 9, 10, 11 \quad \text{and} \quad 0 \leq s \leq 19, \quad (68)$$

always ensuring that they can describe the measured lepton mixing angles at the 3σ level or better for at least one value of the angle θ_N . As expected, we find for combinations m and s both even or odd no dependence of the BRs and CR on the angle θ_S , while for m being even and s odd or vice versa such a dependence exists and is (mainly) determined by $|\cos 2\theta_S|$. Unlike for Case 3 a), this dependence is visible well, similar to the findings for Case 1), see fig. 3. We have, furthermore, checked that results for light neutrino masses with IO are in general similar to those for NO light neutrino masses. For smaller values of m_0 , we can, depending on the choice of the parameters m and s , find a variation of the dependence of the BRs and CR on θ_S . This is similar to what is reported for Case 1), compare figs. 3 and 10. For most of the studied combinations of m and s the BRs of $\mu \rightarrow e\gamma$ and $\mu \rightarrow 3e$ appear to be larger than 10^{-22} and 10^{-23} , respectively, while for e.g. $m = 11$ and $s = 0$ their size can be more suppressed. For $\text{CR}(\mu - e, \text{AI})$ minimum values usually smaller than 10^{-24} can be observed. Regarding the maximal values of the BRs and CR that are found for viable data points, these are similar to those reported for the other cases.

Case 1), $n = 26, s = 1$, NO

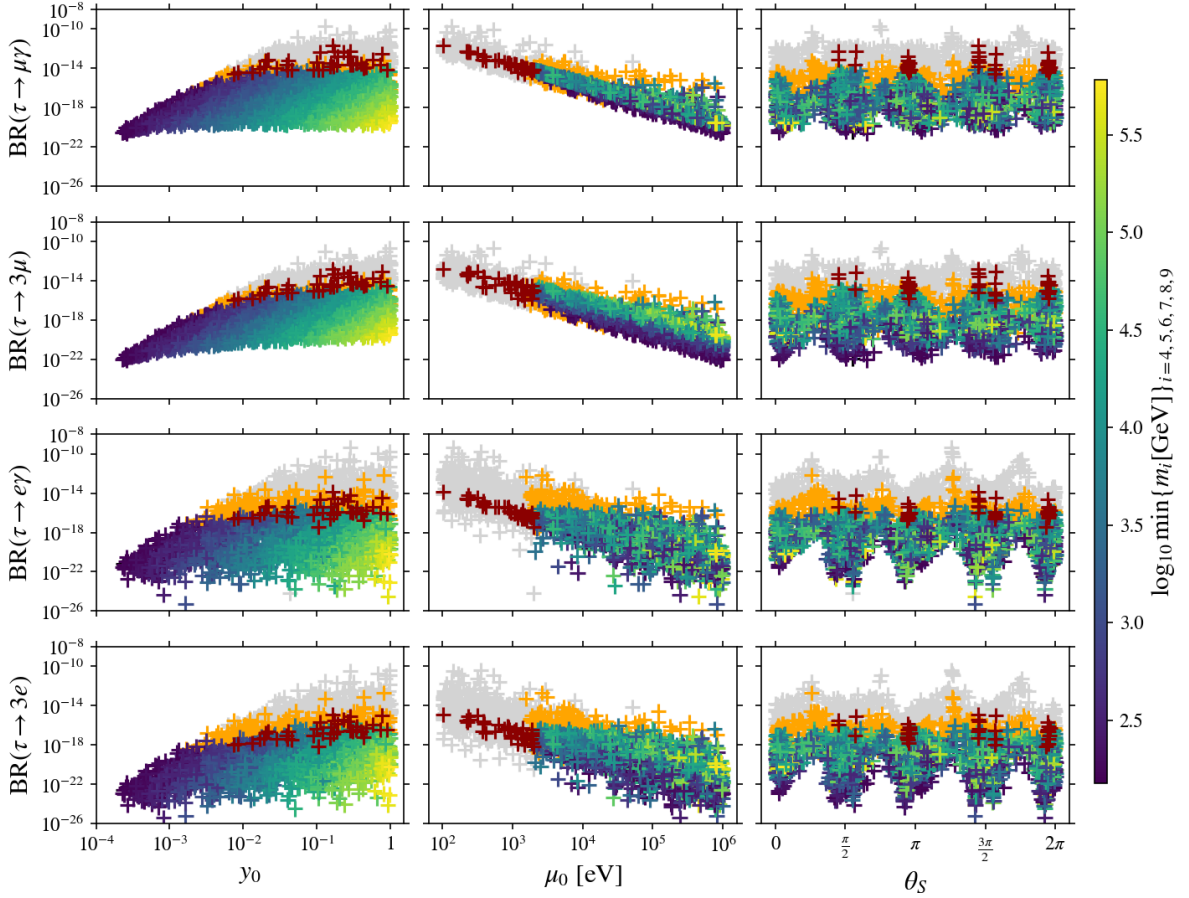


Figure 7: **Case 1).** Results of numerical scan for $\text{BR}(\tau \rightarrow \mu \gamma)$, $\text{BR}(\tau \rightarrow 3 \mu)$, $\text{BR}(\tau \rightarrow e \gamma)$ and $\text{BR}(\tau \rightarrow 3 e)$ varying y_0 , μ_0 and θ_S in the ranges in eqs. (61), (62) and (63), respectively. The parameters n and s are chosen as $n = 26$ and $s = 1$. The light neutrino mass ordering is fixed to NO and m_0 to $m_0 = 0.03 \text{ eV}$. The colour-coding of the data points is the same as in fig. 3.

5.3 Comments on cLFV tau lepton decays

In this section, we briefly comment on the BRs of the four cLFV tau lepton decays $\text{BR}(\tau \rightarrow \mu \gamma)$, $\text{BR}(\tau \rightarrow 3 \mu)$, $\text{BR}(\tau \rightarrow e \gamma)$ and $\text{BR}(\tau \rightarrow 3 e)$. For viable data points (taking into account the current limits on the matrix elements $\eta_{\alpha\beta}$ as well as the future bounds on the three studied $\mu - e$ transitions), the obtained BRs are in general no larger than 10^{-14} and, thus, too small to be observed at Belle II. In most of the analysed situations they are bounded from below by 10^{-23} . For this reason, we just display one set of plots for Case 1), $n = 26$ and $s = 1$, assuming that light neutrino masses follow NO and $m_0 = 0.03 \text{ eV}$, see fig. 7. The plots for IO light neutrino masses look similar. Like for the $\mu - e$ transitions, compare fig. 3, also the BRs of the cLFV tau lepton decays possess a dependence on the angle θ_S . An analogous statement holds for the representatives of the other cases, Case 2) through Case 3 b.1). Furthermore, we note that for the displayed case, the BRs of $\tau \rightarrow e \gamma$ and $\tau \rightarrow 3 e$ can be more suppressed than those for $\tau \rightarrow \mu \gamma$ and $\tau \rightarrow 3 \mu$. Apart from this type of feature, in fig. 13 in appendix A one can observe for Case 3 a), $n = 34, m = 2, s = 2$, light neutrino masses with NO and $m_0 = 10^{-5} \text{ eV}$ that two branches become (slightly) visible (for small y_0), when studying the BRs of $\tau \rightarrow e \gamma$ and $\tau \rightarrow 3 e$. Like for the analysed $\mu - e$ transitions, compare figs. 11 and 12 in the appendix, these branches are associated with the two different values of the angle θ_N which allow to accommodate the lepton mixing angles at the 3σ level or better.

However, such branches cannot be seen in the results for $\text{BR}(\tau \rightarrow \mu \gamma)$ and $\text{BR}(\tau \rightarrow 3 \mu)$.

6 Comparison between the different options

We compare option 3 and its results, studied in this work, with those for option 2, analysed in [49] as well as the ones for option 1, see [37].

Firstly, we remind that the assignment of the different fields under the flavour symmetry can differ for the three options. While LH lepton doublets and RH charged leptons are assigned to the same irreps for all three options, this is not the case for the sterile states N_i and S_j , since they either transform in the same way (for option 1 both as $\mathbf{3}$, while for option 2 both as $\mathbf{3}'$) or as different irreps, $N_i \sim \mathbf{3}$ and $S_j \sim \mathbf{3}'$, for option 3. This is necessary in order to achieve the desired flavour structures of the mass matrices m_D , M_{NS} and μ_S . Furthermore, all fields are assigned to the same charges under $Z_3^{(\text{aux})}$ for the three options.

When comparing option 2 and 3, we note that the form of the matrix M_{NS} in eq. (5) for option 3 is very similar to the one of m_D for option 2 and that the distinction between having the combination in eq. (14) diagonal or only block-diagonal is similar to the discussion for option 2; see also [50] for a setup with type-I seesaw. Indeed, if this combination is diagonal, the result for lepton mixing, compare eq. (23), is analogous to that obtained for the other two options. In case it is only block-diagonal, the angle $\bar{\theta}_N$, defined below eq. (25), corresponds to the effective angle $\bar{\theta}_L$ for option 2. Also the effects of non-unitarity (in lepton mixing), see eqs. (35) and (36), for option 3 are qualitatively similar to the ones observed for option 2, whereas for option 1 the matrix η has a flavour-diagonal and -universal form, leading to the same suppression of all elements of the matrix U_0 , compare eq. (34).

A striking difference between option 3 and the other two options lies in the mass spectrum of the heavy sterile states. While these are all (nearly) degenerate in mass for option 1 and 2, they form three pseudo-Dirac pairs with in general different masses for option 3, see eqs. (13-17) and fig. 1. For light neutrino masses following IO, nevertheless, two of these pairs become close in mass, cf. eq. (46). In addition, due to the choice of the parameter space for option 3, see section 5.1, the masses of the heavy sterile states can vary in a larger range in the numerical scans; in particular, they can be larger (depending on the lightest neutrino mass m_0), while for option 1 and 2 the mass parameter corresponding to the mass scale of the heavy sterile states is always chosen to be no larger than 10 TeV.

Another distinctive feature of option 2 and 3 is the prediction of signal strengths of $\mu \rightarrow e \gamma$, $\mu \rightarrow 3 e$ and $\mu - e$ conversion in aluminium that are in the reach of current/near-future experiments, whereas it has been shown that for option 1 all cLFV signals are very suppressed like in the SM with light neutrino masses. Indeed, the expected rates of the studied cLFV processes, $\text{BR}(\mu \rightarrow e \gamma)$, $\text{BR}(\mu \rightarrow 3 e)$, $\text{CR}(\mu - e, \text{Al})$, $\text{BR}(\tau \rightarrow \mu \gamma)$, $\text{BR}(\tau \rightarrow 3 \mu)$, $\text{BR}(\tau \rightarrow e \gamma)$ and $\text{BR}(\tau \rightarrow 3 e)$, are very similar for option 2 and 3, taking into account the fact that for option 3 the masses of the heavy sterile states can be larger than for option 2 in the numerical scans. Also features, observed for the different cases, Case 1) through Case 3 b.1), are found for both options, e.g. the fact that for Case 1) the results are independent of the parameter s that characterises the CP symmetry, compare section 5.2. In particular, we see that the dependence of the different BRs and the CR on the angle θ_S encountered when studying option 3, see e.g. fig 3, is very similar to the dependence on the angle θ_R for option 2, for all considered cases. Furthermore, the minimum value of μ_0 necessary in order to pass the current bounds on the matrix elements $\eta_{\alpha\beta}$ and the prospective limits on the three analysed $\mu - e$ transitions is typically bounded from below by 2 keV for both options 2 and 3.

However, there are also differences among the results for option 2 and 3. Probably, the most noteworthy one is related to the possible cancellation in $\text{CR}(\mu - e, \text{Al})$. For option 2, such a cancellation always occurs and the value of the mass of the heavy sterile states at which it occurs is universal, i.e. it does not depend on the case, Case 1) through Case 3 b.1), but only on the choice of the nucleus. For option 3, instead we have found that such an exact cancellation does not always exist, e.g. for Case 2) (compare figs. 8 and 9 in appendix A), and if it exists, it can depend

on the chosen case, the group theory parameters as well as μ_0 and the angles θ_N and θ_S . So, a measurement of $\text{CR}(\mu - e, \text{Al})$ in combination with a determination of the mass of (some of) the heavy sterile states could constrain the viable options and/or cases. Additionally, we remark that, in principle, it is possible to also observe a cancellation in one of the BRs for a certain combination of parameters for option 3, compare comments at the end of section 4.2, while this is not the case for option 2. Eventually, for option 3 we can find in some instances two visible branches due to the two different viable values of the angle θ_N , see the numerical scan for Case 3 a), NO light neutrino masses and $m_0 = 10^{-5}$ eV in figs. 11-13 in appendix A. This has not been observed in the analysis of option 2.

7 Summary

We have considered an extension of the SM with 3+3 gauge singlets N_i and S_j . Light neutrino masses are generated with the ISS mechanism. Lepton mixing is determined by a flavour and CP symmetry and their residual groups among charged leptons and the neutral states and, consequently, predicted in terms of one real parameter. In the chosen basis, the charged lepton mass matrix is diagonal and contains three free parameters corresponding to the masses of the electron, muon and tau lepton. Among the neutral states, only the Dirac mass matrix M_{NS} of the gauge singlets N_i and S_j has a non-trivial flavour structure that is fixed by the residual group $G_\nu = Z_2 \times CP$.

There are in total seven real parameters for the neutral states: three mass parameters M_f , $f = 1, 2, 3$, μ_0 the scale of lepton number violation, one Yukawa coupling y_0 and the angles θ_N and θ_S . The light neutrino masses are adjusted with the help of M_f , while θ_N is used in order to achieve lepton mixing angles that agree at the 3σ level or better with experimental data. The three remaining parameters, μ_0 , y_0 and θ_S , are varied in well-motivated ranges in the numerical scans. The heavy sterile states form three pairs of pseudo-Dirac particles with in general distinct masses ranging between 150 GeV and 700 TeV, with the upper limit depending on the value of the lightest neutrino mass m_0 .

In the phenomenological study, we have focussed on the rates of different cLFV processes, in particular $\mu \rightarrow e\gamma$, $\mu \rightarrow 3e$ and $\mu - e$ conversion in nuclei. While current bounds on these and the existing limits on the matrix elements $\eta_{\alpha\beta}$ do not considerably constrain the parameter space, prospective bounds on $\text{BR}(\mu \rightarrow 3e)$ and $\text{CR}(\mu - e, \text{Al})$ impose relevant restrictions. Depending on the case (type of lepton mixing pattern) and the chosen parameters, an exact cancellation in $\text{CR}(\mu - e, \text{Al})$ is possible. In any case, in all analysed examples this CR can reach values as small as 10^{-24} .

Finally, we have compared the results for this variant of the ISS scenario (called option 3) with two other ones (option 1 and 2), studied already in the literature [37, 49], and commented on similarities and important differences. On the one hand, option 1 and 2 predict heavy sterile states that are all (nearly) degenerate in mass, which is not the case for option 3. On the other hand, option 1 leads to very suppressed rates of the cLFV processes, whereas option 2 and 3 can induce sizeable signals. The cancellation in $\text{CR}(\mu - e, \text{Al})$ is exact and universal for option 2 (only depending on the chosen nucleus), but not for option 3. It might, thus, be feasible to at least partly distinguish between these different variants experimentally.

Acknowledgements

We thank Miguel G. Folgado for help with the local computer cluster. This work has been/is supported by the Spanish MINECO through the Ramón y Cajal programme RYC2018-024529-I, the FPI fellowship PRE2021-098730, by the national grant PID2023-148162NB-C21, by the Generalitat Valenciana through PROMETEO/2021/083 as well as by the European Union's Horizon 2020 research and innovation programme under the Marie Skłodowska-Curie Staff Exchange grant agreement No. 101086085 (ASYMMETRY).

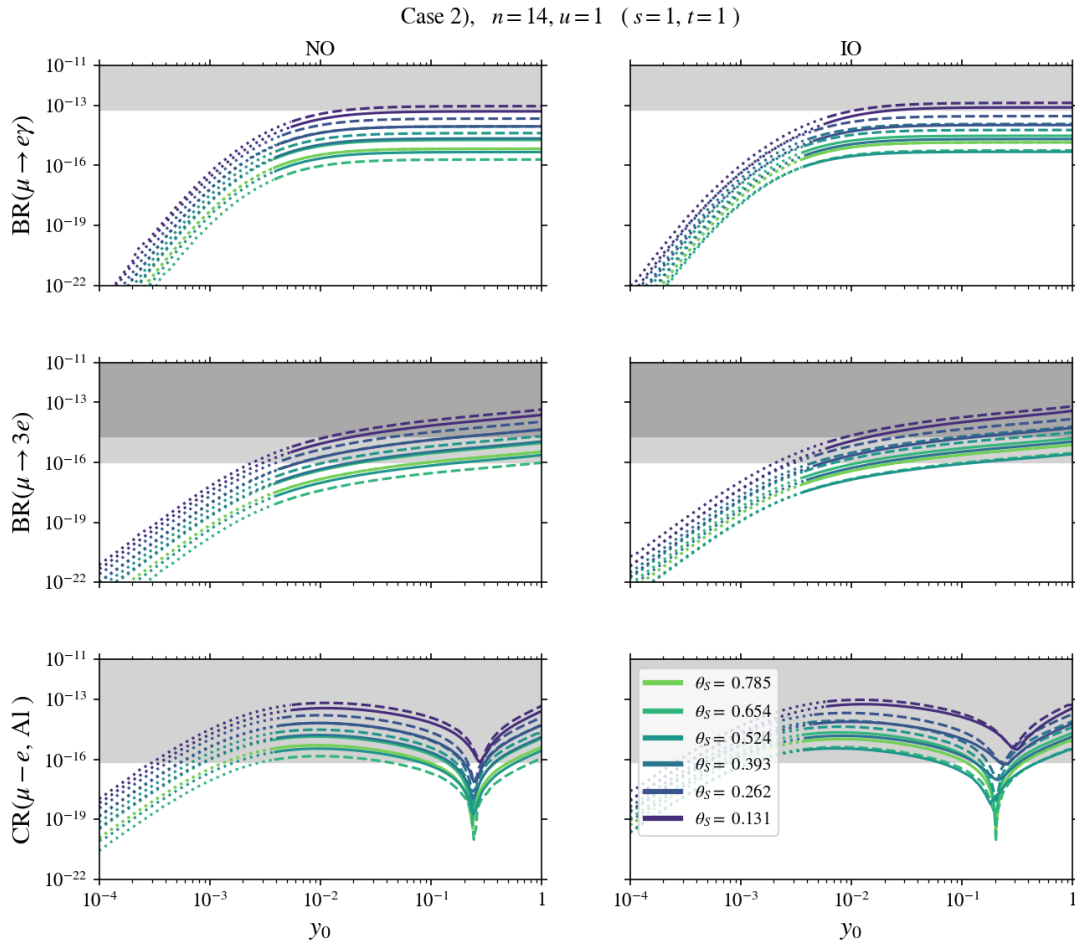


Figure 8: **Case 2).** Results for $\text{BR}(\mu \rightarrow e \gamma)$, $\text{BR}(\mu \rightarrow 3e)$ and $\text{CR}(\mu - e, \text{Al})$ in the upper, middle and lower row, respectively. These results are for $n = 14$, $s = 1$ and $t = 1$ corresponding to $u = 1$ and $v = 3$, and six different values of the angle θ_S , shown in different colours. Results for the two different values of the angle θ_N that lead to a good agreement with the experimental data on lepton mixing are shown with straight and dashed lines, respectively. Otherwise, the conventions are the same as in fig. 2.

A Supplementary plots

In this appendix, we display supplementary plots. Figs. 8 and 9 show results for the BRs of $\mu \rightarrow e \gamma$ and $\mu \rightarrow 3e$ as well as the CR of $\mu - e$ conversion in aluminium for Case 2) and $n = 14$, $s = 1$ and $t = 1$, corresponding to $u = 1$ and $v = 3$. We use the maximal value of the lightest neutrino mass m_0 that is compatible with cosmological measurements in fig. 8, while fixing m_0 to $m_0 = 10^{-5}$ eV in fig. 9. The plots for $n = 14$, $s = 0$ and $t = 1$, corresponding to $u = -1$ and $v = 3$, look similar. With these figures we further illustrate the statements made in section 4.2, where we discuss the BRs and CR analytically.

Fig. 10 displays numerical results for the BRs and the CR for Case 1), $n = 26$ and $s = 1$, assuming that light neutrino masses follow IO and the lightest neutrino mass is set to $m_0 = 10^{-5}$ eV. This figure complements the results that are shown in the main text in fig. 3.

Figs. 11 and 12 show results of numerical scans for the BRs and the CR for Case 3 a), $n = 34$, $m = 2$ and $s = 1$ and $s = 2$, respectively, assuming that light neutrino masses follow NO and the lightest neutrino mass is set to $m_0 = 10^{-5}$ eV. These figures complete the discussion in the main text, in particular the results displayed in fig. 6.

In fig. 13 results for the BRs of the four studied cLFV tau lepton decays $\tau \rightarrow \mu \gamma$, $\tau \rightarrow 3\mu$,

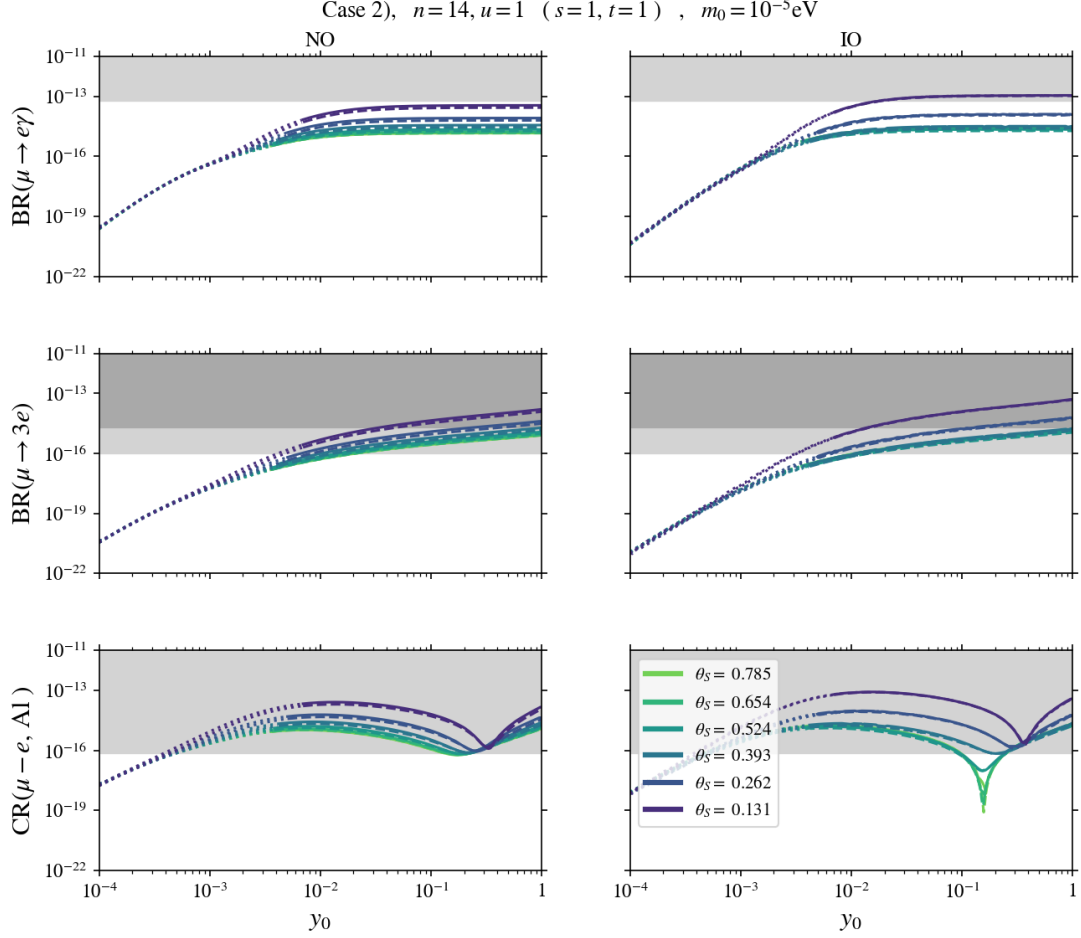


Figure 9: **Case 2).** Results for $\text{BR}(\mu \rightarrow e\gamma)$, $\text{BR}(\mu \rightarrow 3e)$ and $\text{CR}(\mu - e, \text{AI})$ in the upper, middle and lower row, respectively. The lightest neutrino mass m_0 is chosen as $m_0 = 10^{-5}\text{eV}$. The remaining conventions are the same as in fig. 8.

$\tau \rightarrow e\gamma$ and $\tau \rightarrow 3e$ are displayed for Case 3 a), $n = 34, m = 2$ and $s = 2$, light neutrino masses with NO and $m_0 = 10^{-5}\text{eV}$. The plots for IO light neutrino masses look similar, but do not reveal the feature of a (slightly) visible separation of the data points according to the two different viable values of the angle θ_N for the BRs of $\tau \rightarrow e\gamma$ and $\tau \rightarrow 3e$ (for small values of y_0). Fig. 13 supplements the discussion in section 5.3.

Case 1), $n=26$, $s=1$, IO, $m_0=10^{-5}\text{eV}$

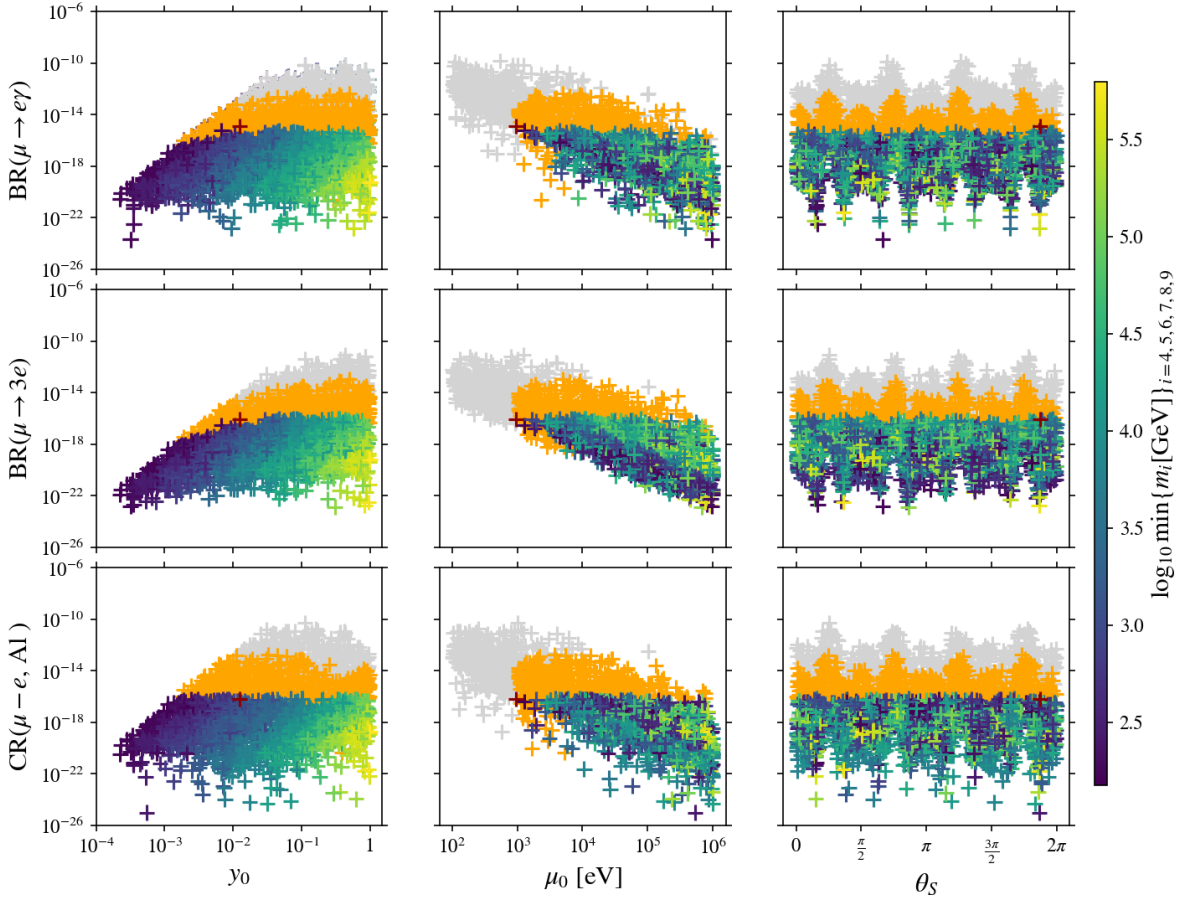


Figure 10: **Case 1).** Results of numerical scan for $\text{BR}(\mu \rightarrow e\gamma)$, $\text{BR}(\mu \rightarrow 3e)$ and $\text{CR}(\mu - e, \text{AI})$ varying y_0 , μ_0 and θ_S in the ranges in eqs. (61), (62) and (63), respectively. The parameters n and s are the same as in fig. 2. The light neutrino mass ordering is fixed to IO and m_0 to $m_0 = 10^{-5}\text{eV}$. The rest of the conventions is the same as in fig. 3.

References

- [1] P. Minkowski, Phys. Lett. B **67** (1977), 421-428.
- [2] T. Yanagida, in *Proceedings of the Workshop on the Unified Theory and the Baryon Number in the Universe* (O. Sawada and A. Sugamoto, eds.), KEK Tsukuba, Japan, 1979, p. 95.
- [3] S. L. Glashow, *The future of elementary particle physics*, in *Proceedings of the 1979 Cargèse Summer Institute on Quarks and Leptons* (M. Lévy, J.-L. Basdevant, D. Speiser, J. Weyers, R. Gastmans, and M. Jacob, eds.), Plenum Press, New York, 1980, pp. 687-713.
- [4] M. Gell-Mann, P. Ramond, and R. Slansky, *Complex spinors and unified theories*, in *Supergravity* (P. van Nieuwenhuizen and D. Z. Freedman, eds.), North Holland, Amsterdam, 1979, p. 315.
- [5] R. N. Mohapatra and G. Senjanovic, Phys. Rev. Lett. **44** (1980) 912.
- [6] M. Magg and C. Wetterich, Phys. Lett. B **94** (1980), 61-64.
- [7] J. Schechter and J. W. F. Valle, Phys. Rev. D **22** (1980), 2227.
- [8] T. P. Cheng and L. F. Li, Phys. Rev. D **22** (1980), 2860.

Case 3 a), $n=34, m=2, s=1, \text{NO}, m_0=10^{-5}\text{eV}$

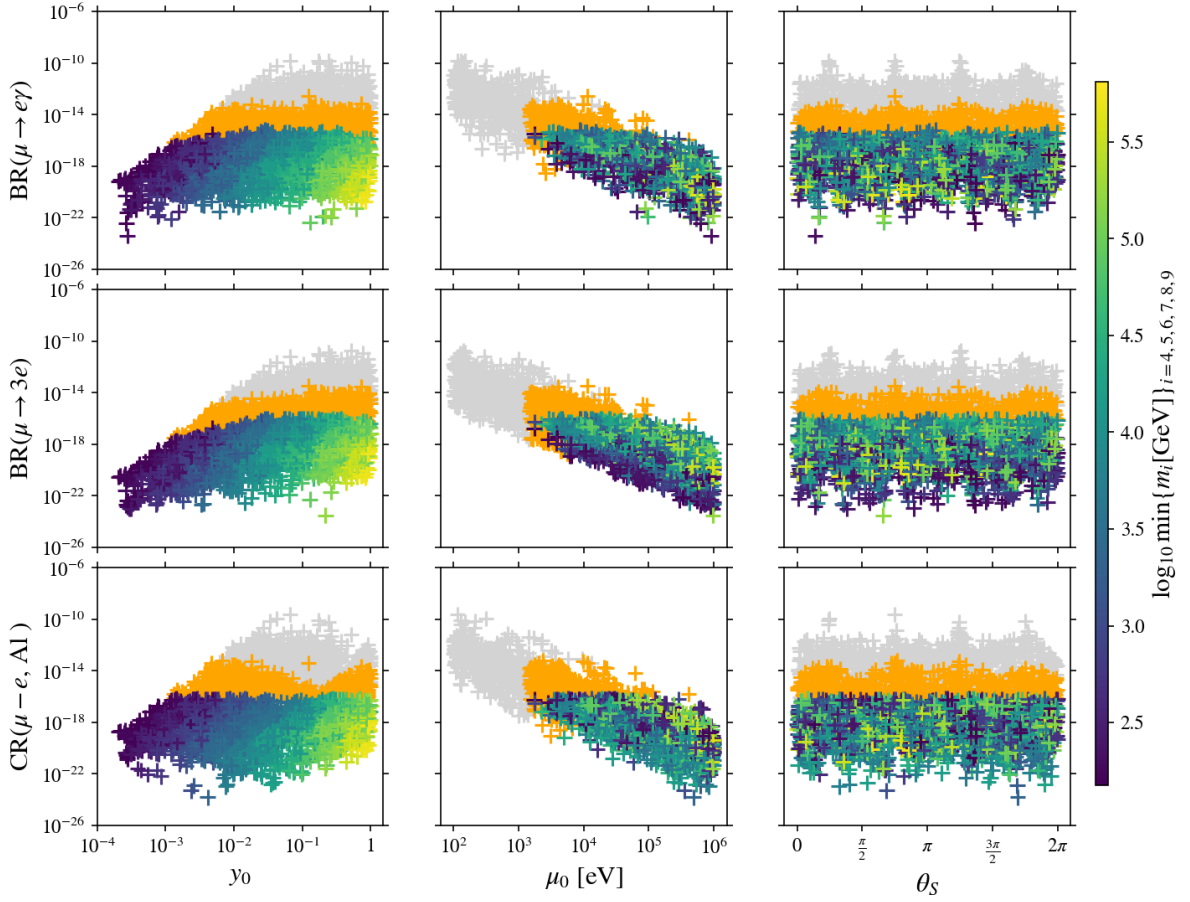


Figure 11: **Case 3 a).** Results of numerical scan for $\text{BR}(\mu \rightarrow e \gamma)$, $\text{BR}(\mu \rightarrow 3 e)$ and $\text{CR}(\mu - e, \text{AI})$ varying y_0 , μ_0 and θ_S in the ranges in eqs. (61), (62) and (63), respectively. The parameters n , m and s are set to $n = 34$, $m = 2$ and $s = 1$. The light neutrino mass ordering is fixed to NO and m_0 to $m_0 = 10^{-5} \text{eV}$. The colour-coding of the data points is the same as in fig. 3.

- [9] G. Lazarides, Q. Shafi and C. Wetterich, Nucl. Phys. B **181** (1981), 287-300.
- [10] C. Wetterich, Nucl. Phys. B **187** (1981), 343-375.
- [11] R. N. Mohapatra and G. Senjanovic, Phys. Rev. D **23** (1981), 165.
- [12] R. Foot, H. Lew, X. G. He and G. C. Joshi, Z. Phys. C **44** (1989), 441.
- [13] M. Shaposhnikov, Nucl. Phys. B **763** (2007), 49-59 [arXiv:hep-ph/0605047 [hep-ph]].
- [14] J. Kersten and A. Y. Smirnov, Phys. Rev. D **76** (2007), 073005 [arXiv:0705.3221 [hep-ph]].
- [15] K. Moffat, S. Pascoli and C. Weiland, arXiv:1712.07611 [hep-ph].
- [16] R. N. Mohapatra and J. W. F. Valle, Phys. Rev. D **34** (1986), 1642.
- [17] R. N. Mohapatra, Phys. Rev. Lett. **56** (1986), 561-563.
- [18] J. Bernabeu, A. Santamaria, J. Vidal, A. Mendez and J. W. F. Valle, Phys. Lett. B **187** (1987), 303-308.
- [19] M. C. Gonzalez-Garcia and J. W. F. Valle, Phys. Lett. B **216** (1989), 360-366.

Case 3 a), $n=34, m=2, s=2, \text{NO}, m_0=10^{-5}\text{eV}$

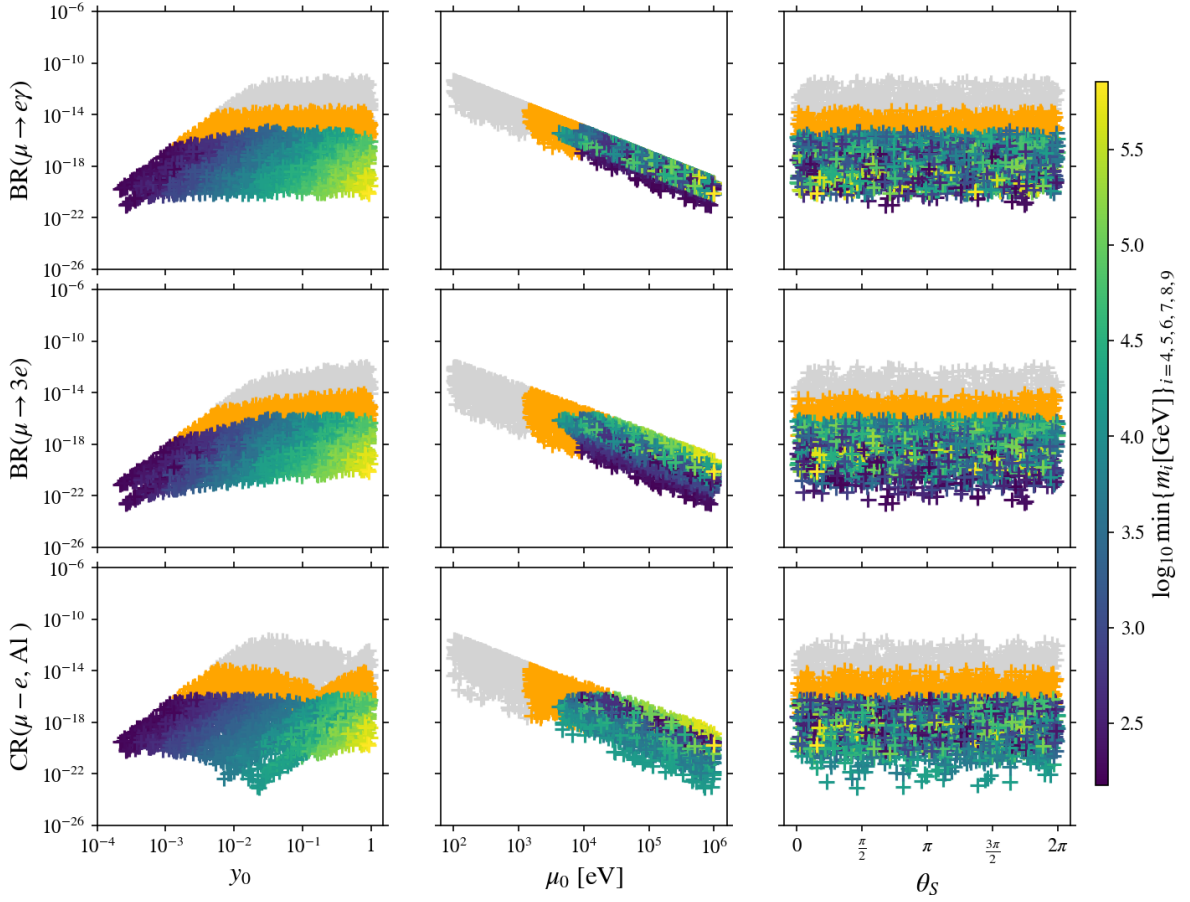


Figure 12: **Case 3 a).** Results of numerical scan for $\text{BR}(\mu \rightarrow e\gamma)$, $\text{BR}(\mu \rightarrow 3e)$ and $\text{CR}(\mu - e, \text{AI})$ varying y_0 , μ_0 and θ_S in the ranges in eqs. (61), (62) and (63), respectively. The parameters n , m and s are set to $n = 34$, $m = 2$ and $s = 2$. The light neutrino mass ordering is fixed to NO and m_0 to $m_0 = 10^{-5}\text{eV}$. The colour-coding of the data points is the same as in fig. 3.

- [20] F. Feruglio, C. Hagedorn and R. Ziegler, JHEP **1307** (2013) 027 [arXiv:1211.5560 [hep-ph]].
- [21] M. Holthausen, M. Lindner and M. A. Schmidt, JHEP **1304** (2013) 122 [arXiv:1211.6953 [hep-ph]].
- [22] M.-C. Chen, M. Fallbacher, K. T. Mahanthappa, M. Ratz and A. Trautner, Nucl. Phys. B **883** (2014) 267 [arXiv:1402.0507 [hep-ph]].
- [23] G. Ecker, W. Grimus and H. Neufeld, Nucl. Phys. B **247** (1984) 70.
- [24] G. Ecker, W. Grimus and H. Neufeld, J. Phys. A **20** (1987) L807.
- [25] H. Neufeld, W. Grimus and G. Ecker, Int. J. Mod. Phys. A **3** (1988) 603.
- [26] W. Grimus and M. N. Rebelo, Phys. Rept. **281** (1997) 239 [arXiv:hep-ph/9506272].
- [27] P. F. Harrison and W. G. Scott, Phys. Lett. B **535** (2002) 163 [arXiv:hep-ph/0203209].
- [28] W. Grimus and L. Lavoura, Phys. Lett. B **579** (2004) 113 [arXiv:hep-ph/0305309].
- [29] S. F. King, J. Phys. G **42** (2015), 123001 [arXiv:1510.02091 [hep-ph]].

Case 3 a), $n=34, m=2, s=2, \text{NO}, m_0=10^{-5}\text{eV}$

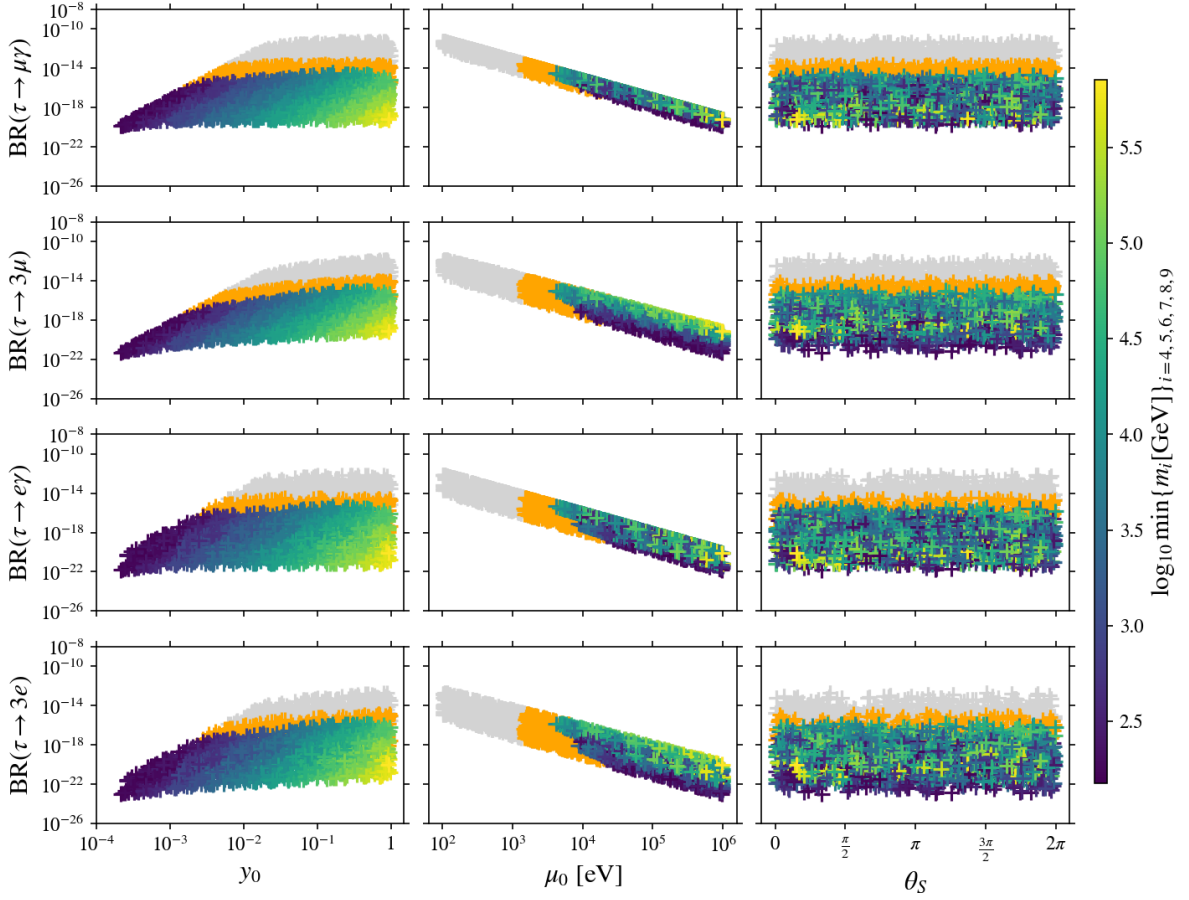


Figure 13: **Case 3 a).** Results of numerical scan for $\text{BR}(\tau \rightarrow \mu \gamma)$, $\text{BR}(\tau \rightarrow 3 \mu)$, $\text{BR}(\tau \rightarrow e \gamma)$ and $\text{BR}(\tau \rightarrow 3 e)$ varying y_0 , μ_0 and θ_S in the ranges in eqs. (61), (62) and (63), respectively. The parameters n , m and s are set to $n = 34$, $m = 2$ and $s = 2$. The light neutrino mass ordering is fixed to NO and m_0 to $m_0 = 10^{-5}\text{eV}$. The colour-coding of the data points is the same as in fig. 3.

- [30] F. Feruglio and A. Romanino, Rev. Mod. Phys. **93** (2021) no.1, 015007 [arXiv:1912.06028 [hep-ph]].
- [31] H. Ishimori, T. Kobayashi, H. Ohki, Y. Shimizu, H. Okada and M. Tanimoto, Prog. Theor. Phys. Suppl. **183** (2010), 1-163 [arXiv:1003.3552 [hep-th]].
- [32] T. Kobayashi, H. Ohki, H. Okada, Y. Shimizu and M. Tanimoto, *An Introduction to Non-Abelian Discrete Symmetries for Particle Physicists*, 2022, ISBN 978-3-662-64678-6, 978-3-662-64679-3.
- [33] W. Grimus and P. O. Ludl, J. Phys. A **45** (2012), 233001 [arXiv:1110.6376 [hep-ph]].
- [34] C. Luhn, S. Nasri and P. Ramond, J. Math. Phys. **48** (2007), 073501 [arXiv:hep-th/0701188 [hep-th]].
- [35] J. A. Escobar and C. Luhn, J. Math. Phys. **50** (2009), 013524 [arXiv:0809.0639 [hep-th]].
- [36] C. Hagedorn, A. Meroni and E. Molinaro, Nucl. Phys. B **891** (2015), 499-557 [arXiv:1408.7118 [hep-ph]].

- [37] C. Hagedorn, J. Kriewald, J. Orloff and A. M. Teixeira, *Eur. Phys. J. C* **82** (2022) no.3, 194 [arXiv:2107.07537 [hep-ph]].
- [38] G. J. Ding, S. F. King and T. Neder, *JHEP* **1412** (2014) 007 [arXiv:1409.8005 [hep-ph]].
- [39] G. J. Ding and S. F. King, *Phys. Rev. D* **93** (2016) 025013 [arXiv:1510.03188 [hep-ph]].
- [40] S. F. King and T. Neder, *Phys. Lett. B* **736** (2014) 308 [arXiv:1403.1758 [hep-ph]].
- [41] G. J. Ding, S. F. King, C. Luhn and A. J. Stuart, *JHEP* **1305** (2013) 084 [arXiv:1303.6180 [hep-ph]].
- [42] F. Feruglio, C. Hagedorn and R. Ziegler, *Eur. Phys. J. C* **74** (2014) 2753 [arXiv:1303.7178 [hep-ph]].
- [43] G. J. Ding, S. F. King and A. J. Stuart, *JHEP* **1312** (2013) 006 [arXiv:1307.4212 [hep-ph]].
- [44] C. C. Li and G. J. Ding, *Nucl. Phys. B* **881** (2014) 206 [arXiv:1312.4401 [hep-ph]].
- [45] C. C. Li and G. J. Ding, *JHEP* **1508** (2015) 017 [arXiv:1408.0785 [hep-ph]].
- [46] G. J. Ding and Y. L. Zhou, *Chin. Phys. C* **39** (2015) 2, 021001 [arXiv:1312.5222 [hep-ph]].
- [47] G. J. Ding and Y. L. Zhou, *JHEP* **1406** (2014) 023 [arXiv:1404.0592 [hep-ph]].
- [48] G. J. Ding and S. F. King, *Phys. Rev. D* **89** (2014) 9, 093020 [arXiv:1403.5846 [hep-ph]].
- [49] F. P. Di Meglio and C. Hagedorn, *Nucl. Phys. B* **1018** (2025), 117020 [arXiv:2407.19734 [hep-ph]].
- [50] M. Drewes, Y. Georis, C. Hagedorn and J. Klarić, *JHEP* **12** (2022), 044 [arXiv:2203.08538 [hep-ph]].
- [51] H. Hettmansperger, M. Lindner and W. Rodejohann, *JHEP* **04** (2011), 123 [arXiv:1102.3432 [hep-ph]].
- [52] I. Esteban, M. C. Gonzalez-Garcia, M. Maltoni, I. Martinez-Soler, J. P. Pinheiro and T. Schwetz, *JHEP* **12** (2024), 216 [arXiv:2410.05380 [hep-ph]].
- [53] N. Aghanim *et al.* [Planck], *Astron. Astrophys.* **641** (2020), A6 [erratum: *Astron. Astrophys.* **652** (2021), C4] [arXiv:1807.06209 [astro-ph.CO]].
- [54] R. Alonso, M. Dhen, M. B. Gavela and T. Hambye, *JHEP* **01** (2013), 118 [arXiv:1209.2679 [hep-ph]].
- [55] A. Ilakovac and A. Pilaftsis, *Nucl. Phys. B* **437** (1995), 491 [arXiv:hep-ph/9403398].
- [56] R. Kitano, M. Koike and Y. Okada, *Phys. Rev. D* **66** (2002), 096002 [erratum: *Phys. Rev. D* **76** (2007), 059902] [arXiv:hep-ph/0203110 [hep-ph]].
- [57] F. del Aguila and J. A. Aguilar-Saavedra, *Nucl. Phys. B* **813** (2009), 22-90 [arXiv:0808.2468 [hep-ph]].
- [58] F. del Aguila and J. A. Aguilar-Saavedra, *Phys. Lett. B* **672** (2009), 158-165 [arXiv:0809.2096 [hep-ph]].
- [59] C. Y. Chen and P. S. B. Dev, *Phys. Rev. D* **85** (2012), 093018 [arXiv:1112.6419 [hep-ph]].
- [60] A. Das and N. Okada, *Phys. Rev. D* **88** (2013), 113001 [arXiv:1207.3734 [hep-ph]].
- [61] A. Abada and M. Lucente, *Nucl. Phys. B* **885** (2014), 651-678 [arXiv:1401.1507 [hep-ph]].

- [62] E. Arganda, M. J. Herrero, X. Marcano and C. Weiland, *Phys. Rev. D* **91** (2015) no.1, 015001 [arXiv:1405.4300 [hep-ph]].
- [63] A. Abada, V. De Romeri and A. M. Teixeira, *JHEP* **09** (2014), 074 [arXiv:1406.6978 [hep-ph]].
- [64] A. Abada, M. E. Krauss, W. Porod, F. Staub, A. Vicente and C. Weiland, *JHEP* **11** (2014), 048 [arXiv:1408.0138 [hep-ph]].
- [65] A. Abada, V. De Romeri, S. Monteil, J. Orloff and A. M. Teixeira, *JHEP* **04** (2015), 051 [arXiv:1412.6322 [hep-ph]].
- [66] E. Arganda, M. J. Herrero, X. Marcano and C. Weiland, *Phys. Rev. D* **93** (2016) no.5, 055010 [arXiv:1508.04623 [hep-ph]].
- [67] A. Abada, V. De Romeri and A. M. Teixeira, *JHEP* **02** (2016), 083 [arXiv:1510.06657 [hep-ph]].
- [68] V. De Romeri, M. J. Herrero, X. Marcano and F. Scarcella, *Phys. Rev. D* **95** (2017) no.7, 075028 [arXiv:1607.05257 [hep-ph]].
- [69] S. Antusch, E. Cazzato and O. Fischer, *Int. J. Mod. Phys. A* **32** (2017) no.14, 1750078 [arXiv:1612.02728 [hep-ph]].
- [70] A. Crivellin, F. Kirk and C. A. Manzari, *JHEP* **12** (2022), 031 [arXiv:2208.00020 [hep-ph]].
- [71] A. Abada and T. Toma, *JHEP* **08** (2024), 128 [arXiv:2405.01648 [hep-ph]].
- [72] M. Blennow, E. Fernández-Martínez, J. Hernández-García, J. López-Pavón, X. Marcano and D. Naredo-Tuero, *JHEP* **08** (2023), 030 [arXiv:2306.01040 [hep-ph]].
- [73] K. Afanaciev *et al.* [MEG II], *Eur. Phys. J. C* **85** (2025) no.10, 1177 [erratum: *Eur. Phys. J. C* **85** (2025) no.11, 1317] [arXiv:2504.15711 [hep-ex]].
- [74] U. Bellgardt *et al.* [SINDRUM], *Nucl. Phys. B* **299** (1988), 1-6.
- [75] W. H. Bertl *et al.* [SINDRUM II], *Eur. Phys. J. C* **47** (2006), 337-346.
- [76] P. Wintz, *Prepared for 29th International Conference on High-Energy Physics (ICHEP 98), Vancouver, Canada, 23-29 Jul 1998.*
- [77] A. M. Baldini *et al.* [MEG II], *Symmetry* **13** (2021) no.9, 1591 [arXiv:2107.10767 [hep-ex]].
- [78] A. Blondel, A. Bravar, M. Pohl, S. Bachmann, N. Berger, M. Kiehn, A. Schoning, D. Wiedner, B. Windelband, P. Eckert *et al.*, arXiv:1301.6113 [physics.ins-det].
- [79] R. Abramishvili *et al.* [COMET], *PTEP* **2020** (2020) no.3, 033C01 [arXiv:1812.09018 [physics.ins-det]].
- [80] A. Jansen [COMET], *EPJ Web Conf.* **282** (2023), 01014.
- [81] L. Bartoszek *et al.* [Mu2e], arXiv:1501.05241 [physics.ins-det].
- [82] M. Artuso, R. H. Bernstein, A. A. Petrov, T. Blum, A. Di Canto, S. Davidson, B. Echenard, S. Gori, E. Goudzovski, R. F. Lebed *et al.*, arXiv:2210.04765 [hep-ex].
- [83] A. Abdesselam *et al.* [Belle], *JHEP* **10** (2021), 19 [arXiv:2103.12994 [hep-ex]].
- [84] P. A. Zyla *et al.* [Particle Data Group], *PTEP* **2020** (2020) no.8, 083C01.
- [85] I. Adachi *et al.* [Belle II], *JHEP* **09** (2024), 062 [arXiv:2405.07386 [hep-ex]].
- [86] R. Aaij *et al.* [LHCb], arXiv:2601.20785 [hep-ex].
- [87] S. Banerjee, V. Cirigliano, M. Dam, A. Deshpande, L. Fiorini, K. Fuyuto, C. Gal, T. Husek, E. Mereghetti, K. Monsálvez-Pozo *et al.*, arXiv:2203.14919 [hep-ph].